Maria da Piedade Oom de Albuquerque d'Orey

Bachelor of Science in Applied Chemistry

Functionalization of Silica Surfaces: Influence in Naproxen Molecular Mobility and Release Profile

Dissertation to obtain the degree of Master in Bioorganic Chemistry

Supervisor: Dr. Teresa Cordeiro, FCT/UNL

Co-Supervisor: Prof. Doutora Madalena Dionísio Andrade, FCT/UNL

Jury:

President: Prof. Doutora Paula Cristina de Sério Branco

Arguing: Prof. Doutora Maria Margarida Canas Mendes de Almeida Cardoso

FACULDADE DE CIÊNCIAS E TECNOLOGIA
UNIVERSIDADE NOVA DE LISBOA

October 2018

Maria da Piedade Oom de Albuquerque d'Orey

Bachelor of Science in Applied Chemistry

Functionalization of Silica Surfaces: Influence in Naproxen Molecular Mobility and Release Profile

Dissertation to obtain the degree of Master in Bioorganic Chemistry

Supervisor: Dr. Teresa Cordeiro, FCT/UNL

Functionalization of Silica Surfaces: Influence in Naproxen Molecular Mobility and Release Profile

Acknowledgements:

The assignment I developed was of great interest to me, as it was chemistry applied to the pharmaceutical area. I acquired new skills, and increased my understanding on the subject.

As so, I would like to thank my supervisor, Dr. Teresa Cordeiro, for all the help, time and support through this year she gave me.

I would also like to thank my co-supervisor, Prof. Doutora Madalena Dionísio for the opportunity to work in this project, and for all the time and effort to teach me.

Thank you to all the people that helped me during my laboratory work:

- Professor Doutor João Sotomayor with the drug loading.
- Professora Doutora Margarida Cardoso with laboratory facilities for drug delivery.
- Professora Doutora Marta Corvo with NMR analysis and data treatment.
- Doutora Inês Matos for the aid in the silica synthesis and silica surface functionalization
- Dr. Nuno Costa from Laboratório de Análises (FCT-UNL) for textural characterization of the silica.
- D. Idalina, D. Conceição e D. Palminha for the availability to aid with laboratory equipment.

Thanks too, to my laboratory colleagues Andreia Santos and Sara Inocêncio, for all the encouragement.

At last, I would like to thank my parents, my two brothers, family and friends for all their support in this final stage of my studies.

Abstract:

This work aimed to improve aqueous drug solubility by amorphization upon loading in silica porous matrixes and stabilize it in the amorphous form. Naproxen was chosen as the target material, a practically insoluble pharmaceutical drug, with anti-pyretic and anti-inflammatory properties. To evaluate the influence of guest-host interactions in the drug delivery, two silica matrixes were synthesized differing in their surface composition: unmodified MCM-41 mainly with surface silanol groups and MCM-41_Func caped with methyl groups. The surface area modification with methyl groups was confirmed by attenuated total reflectance Fourier transform infrared spectroscopy (ATR-FTIR), thermogravimetric analysis (TGA) and nuclear magnetic resonance (NMR). Textural analysis showed narrow pore diameter distributions centered at 3.0 and 2.9 nm, respectively.

To evaluate the guest's physical state, different techniques were used as: differential scanning calorimetry (DSC), dielectric relaxation spectroscopy (DRS) and attenuated total reflectance Fourier transform infrared (ATR-FTIR) spectroscopy. These analyses showed that naproxen was successful incorporated in the both silica. The naproxen's amorphization was confirmed by the DSC detection of the glass transition, located in between ~0ºC and 22ºC. However, crystallization and melting are always observed, nonetheless in low extent (~6 % of crystallization degree).

The mobility of the amorphous pharmaceutical drug incorporated inside these silica pores, was probed by DRS, allowing estimating a dielectric glass transition temperature in good agreement with the calorimetric one and revealing a higher mobility for the hydrated unmodified composite. It was shown that this mobility enhancement controls the drug delivery, monitored by ultraviolet spectroscopy, which revealed to be faster in the unmodified matrix.

The studied composites show promising behavior as controlled drug delivery systems.

Keywords: Naproxen, Inorganic Silica, Amorphous, Glass Transition, Control Release.

Resumo:

Este trabalho teve como objetivo melhorar a solubilidade aquosa de um fármaco, por amorfização através de incorporação em matrizes porosas de sílica, e estabilizá-lo na forma amorfa. O naproxeno foi escolhido como material alvo, sendo um fármaco praticamente insolúvel, exibindo propriedades ant-ipiréticas e anti-inflamatórias. Para avaliar a influência das interações hóspede-hospedeiro na libertação do fármaco, foram sintetizadas duas matrizes de sílica diferindo na sua composição superficial: uma não modificada, MCM-41, tento sobretudo grupos superficiais to tipo silanol, e uma modificada, por metilação MCM-41_Func. A modificação da área superficial com grupos metilo foi confirmada por espectroscopia de infravermelho com refletância total atenuada por transformada de Fourier (ATR-FTIR), análise termogravimétrica e ressonância magnética nuclear. A análise textural mostrou distribuições de diâmetro de poro estreitas centradas em 3,0 e 2,9 nm, respectivamente.

Para avaliar o estado físico do naproxeno incorporado, foram utilizadas diferentes técnicas tais como: calorimetria diferencial de varrimento (DSC), espectroscopia de relaxação dielétrica (DRS) e ATR-FTIR. Estas análises mostraram que o naproxeno foi incorporado com sucesso em ambas as sílicas. A amorfização do naproxeno foi confirmada por DSC através da detecção da transição vítrea, localizada entre ~ 0ºC e 22ºC. No entanto, observa-se sempre cristalização e fusão, ainda que em baixa extensão (~ 6% de grau de cristalização).

A mobilidade do fármaco amorfo incorporado dentro destes poros de sílica, foi sondada por DRS, permitindo estimar uma temperatura dielétrica de transição vítrea em boa concordância com a temperatura calorimétrica, e revelando uma maior mobilidade para o compósito hidratado não modificado. Demonstrou-se que este aumento de mobilidade controla a libertação do fármaco que se mostrou mais rápida na matriz não modificada; a libertação do naproxeno foi monitorizada por espectroscopia de ultravioleta,.

Os compósitos estudados apresentam comportamento promissor para aplicação como sistemas controlados de liberação de fármacos.

Palavras-Chave: Naproxeno, Sílica Inorgânica, Amorfo, Transição Vítrea, Libertação Controlada.

TABLE OF CONTENTS:

1 Introduction 1
1.1 Motivation 1
1.2 Naproxen 1
1.3 Bioavailability and Biopharmaceutics Classification System (BCS) 2
1.4 Crystals and Amorphous Materials 3
1.5 Phase Transitions 5
1.5.1 Melting 6
1.5.2 Glass Transitions 6
1.6 Silica MCM-41 8
1.7 Techniques 8
1.7.1 Attenuated Total Reflectance Fourier Transform Infrared Spectroscopy (ATR-FTIR) 8
1.7.2 Thermogravimetric Analysis (TGA) 10
1.7.3 Scanning Electron Microscopy (SEM) 11
1.7.4 Transmission Electron Microscopy (TEM) 11
1.7.5 Differential Scanning Calorimetry (DSC) 11
1.7.6 Nuclear Magnetic Resonance (NMR) 13
1.7.7 Dielectric Relaxation Spectroscopy (DRS) 14
1.7.8 Ultraviolet Spectroscopy (UV-Vis) 18
2 Methods and Materials 19
2.1 Synthesis of Mesoporous MCM-41 19
2.2 Functionalization of the Mesoporous Silica MCM-41 20
2.3 Textural analyses of MCM-41 and MCM-41 Functionalized by Nitrogen Absorption Analysis 20
2.4 Drug Loading 21
2.5 Scanning Electron Microscopy (SEM) 22
2.6 Transmittance Electron Microscopy (TEM) 22
2.7 Thermogravimetric Analyses (TGA) 22
2.8 Attenuated Total Reflectance Fourier Transform Infrared Spectroscopy (ATR-FTIR) 23
2.9 Nuclear Magnetic Resonance (NMR) 23
2.10 Different Scanning Calorimetry (DSC) 23
2.11 Dielectric Relaxation Spectroscopy (DRS) 25
2.12 Control Release Experiments 26
2.13 Ultraviolet-Visible Spectroscopy (UV-VIS Spectroscopy) 27
3 Results and Discussion 29
3.1 Scanning Electron Microscopy (SEM) 29

3.2 Transmission Electron Microscopy (TEM) 30
3.3 Thermogravimetric Analysis (TGA) 31
3.4 Attenuated Total Reflectance Fourier Transform Infrared Spectroscopy (ATR-FTIR) 33
3.5 Nuclear Magnetic Resonance (NMR) 37
3.6 Different Scanning Calorimetry (DSC) 39
3.7 Dielectric Relaxation Spectroscopy (DRS) 49
3.8 Control Release Experiments 55
4 Conclusion 57
5 References 59
6 Anexes 63

LIST OF FIGURES:

Figure 1. Representation of naproxen molecular structure. * indication of the chiral centre. 2
Figure 2. Amorphous solids vs Crystalline solids. 3
Figure 3. Demonstration of nucleation rate, $J_{nucleation}$, and rate of crystal growth, J_{growth}, in respect to temperature. T_g is the glass-transition temperature, T_m is the melting temperature, units are arbitrary for rate. The area where the curves overlap, in grey, is the temperature range where nucleation and growth happen.[15] 4
Figure 4. Thermodynamic properties changes in a) first order phase transitions and b) second order phase transitions[16] 5
Figure 5. Representation of T_g from a DSC scan, idientification of onset, midpoint and offset or endset. 7
Figure 6. Representation of temperature dependence on enthalpy and volume. T_{ga} is the glass transition temperature formed from a slow cooling rate and T_{gb} from a faster. T_m is the melting temperature.[19] 7
Figure 7. Scheme of a multiple reflection in ATR-FTIR.[27] 10
Figure 8. Diagram representation of the heat-flux of differential scanning calorimetry.[32] 12
Figure 9. Differential Scanning Calorimetry profile with exothermic and endothermic heat flow plotted versus temperature.[33] 13
Figure 10. Attributed Q^n nomenclature to the different silanol groups on the silica surface.[36] 14
Figure 11. Frequency response of the dielectric mechanisms.[38] 15
Figure 12. Representation of electronic transitions that results from light absortion.[42] 18
Figure 13. Representation scheme of the MCM-41 synthesis.[22] 19
Figure 14. Representation of MCM-41 functionalization. Adapted[43] 20
Figure 15. Assembly line for drug loading process. 21
Figure 16. Illustration of how the temperatures are extracted at onset, midpoint and endset of glass transition. 24
Figure 17. Thermal treatment applied to a) native naproxen and b) both silicas, in red heating cycles and in blue cooling cycles. 24
Figure 18. First Thermal treatment applied to both loaded composites in red heating cycles, in blue cooling cycles and in green annealing cycle. 25
Figure 19. Thermal treatment applied to a) MCM-41 loaded with naproxen, b) MCM-41_Func loaded with naproxen, in red heating cycles, in blue cooling cycles and in green annealing cycles. 25
Figure 20. Naproxen UV-Vis spectrum 27
Figure 21. SEM Images of unloaded MCM-41. On the left, the image with an amplification of 200x and on right with 10.000x. 29
Figure 22. SEM images of loaded MCM-41. Top left 200x, top right 2.000x, bottom left 5.000x and bottom right 10.000x amplification. 29
Figure 23. TEM micrographs of unloaded MCM-41. 30
Figure 24.TEM micrographs of loaded MCM-41 with naproxen. 30
Figure 25. TGA plots for native naproxen (orange), both unloaded MCM-41(dark blue) and MCM-41_Func (light green) and the respective composites (light blue and dark green). 31
Figure 26. Derivative plot of native naproxen (orange), both loaded MCM-41 (bluw) and MCM-41_Func (green). 32
Figure 27. Region of the spectrum between 4000 and 3500 cm^{-1} for both matrixes, in blue the unmodified and in green the modified one. All the curves were vertically displaced for a better visualization. The dashed lines included to aid band visualization. 34

Figure 28. Region of the spectrum between 3600 and 1200 cm^{-1} for both silica, in blue the unmodified and in green the modified one. All the curves were vertically displaced for a better visualization. The dashed lines to aid band visualization. ... 34
Figure 29. Region of the spectrum between 1400 and 400 cm^{-1} for the two matrixes, in green the unmodified and in blue the modified one. All the curves were vertically displaced for a better visualization. The dashed lines to aid band visualization. ... 35
Figure 30. ATR-FTIR spectrum in the C-H, C=C and C=O regions for a comparison of native naproxen with the loaded and unloaded Matrixes of MCM-41 at room temperature. All the curves were displaced vertically for a better comprehension and visualization. ... 36
Figure 31. ^{29}Si MAS NMR spectra of the unloaded silica matrixes (see legend). ... 37
Figure 32. ^{13}C NMR spectra of MCM-41 and MCM-41_Func. ... 38
Figure 33. Thermogram of native naproxen, main cycles represented. In pink the first heating cycle followed by de second cooling cycle in blue. ... 39
Figure 34. Thermogram of unloaded a) MCM-41 and b) MCM-41_Func, main cycles represented. In dark pink the first heating, second cooling cycle in blue followed by the second heating cycle in lighter pink. ... 40
Figure 35. Thermogram of loaded MCM-41, main cycles represented. In dark pink the first heating cycle and native naproxen heating cycle, the second cooling cycle in blue, second heating cycle in lighter pink followed by the cycle after annealing in purple. Native naproxen curve in orange was displaced vertically for a better comprehension and visualization. ... 41
Figure 36. Thermogram of loaded MCM-41_Naproxen two months after the first reading, main cycles represented. In dark pink the first heating cycle, the second cooling cycle in blue, second heating cycle in purple. ... 42
Figure 37. Thermogram of loaded MCM-41, main cycles represented. In dark pink the first heating cycle, in orange native naproxen heating cycle, the second cooling cycle in blue, heating cycle after annealing in dark blue, heating cycle after second annealing in purple, seventh cooling cycle in green. Native naproxen curve was displaced vertically for a better comprehension and visualization. ... 42
Figure 38. Thermogram of loaded MCM-41, derivative plot evidencing one populations, smoothing was applied (x15). ... 44
Figure 39. Thermogram of loaded functionalized MCM-4, main cycles represented. In dark pink the first heating cycle and native naproxen heating cycle, the second cooling cycle in blue, second heating cycle in lighter pink followed by the cycle after annealing in purple. Native naproxen curve in orange was displaced vertically for a better comprehension and visualization. ... 44
Figure 40. Thermogram of loaded functionalized MCM-41, main cycles represented. In dark pink the first heating cycle, in orange native naproxen heating cycle, the second cooling cycle in blue, heating cycle after annealing in dark blue, second heating cycle after annealing in purple, seventh cooling cycle in green. Native naproxen curve was displaced vertically for a better comprehension and visualization. ... 45
Figure 41. Thermogram of loaded MCM-41_Func_Nap, derivative plot evidencing one populations, smoothing was applied (x15). ... 46
Figure 42. Comparison of both composites, after annealing (dried); a) T_g plot and b) derivative plot of T_g. In blue unmodified composite and in green functionalized composite. ... 48
Figure 43. Dielectric loss spectra taken isothermally at the temperatures indicated for a) and b) hydrated (1^{st} heating) and c) and d) dried (2^{nd} heating) composites; see legend inside figure. ... 49
Figure 44. Isochronal plots at the frequency 1x104 Hz for composites, a) unmodified matrix and b) modified matrix. In blue hydrated cycle (1^{st} heating) and in red, dried cycle (2^{nd} heating). ... 50

Figure 45. Comparative analyses between both composites for first and second heating cycles, through isochronal a), b) and isothermal c), d) representations. ... 51
Figure 46. Representation of a fitting process. 52
Figure 47. Relaxation time, τ, versus 1/T for the alpha process of the composite MCM-41, pink circles, isothermal loss data, blue circles, τ obtained from isochronal plots for some frequencies ($\tau=1/(2\pi f)$, $1/T_{max}$). The solid line is the VFTH fit to the data (see equation 7, and parameters in table 11). Arrows indicating dielectric $T_{g,DRS}$ (τ=100 s) and calorimetric $T_{g,DSC(onset)}$ glass transition temperatures. 53
Figure 48. Normalized drug release and dissolution profiles in a pH= 6.8 media..... 55

LIST OF TABLES:

Table 1. Representation of the Biopharmaceutics Classification System. [11] 3
Table 2. Textural properties of MCM-41 and MCM-41 functionalized. 21
Table 3. Temperature steps and range of dielectric measurements at which isothermal spectra were collected for both composites. 26
Table 4. Water content, organic functional groups and loading percentages for both silica and composites. 33
Table 5. Percentage and Chemical shifts of deconvoluted ^{29}Si MAS NMR spectra of MCM-41 and MCM-41_Func.[25] 38
Table 6. Table showing values of enthalpy variation and melting temperature for MCM-41 incorporated with naproxen with no framework, the following values are an average from three collections. 41
Table 7. Values of thermal transitions collected from DSC for unmodified loaded composite, MCM-41_Naproxen. The data result from an average of three collections. 43
Table 8. Table showing values of enthalpy variation and melting temperature for functionalized MCM-41 incorporated with naproxen. The values result from an average of three collections. 45
Table 9. Values of thermal transitions collected from DSC for modified loaded composite, MCM-41_Naproxen. The data resulted from an average of three collections. 46
Table 10. Crystalline Percentage calculi for both loaded matrixes. 47
Table 11. Estimated parameters of the VFTH Fit to the relaxation times of the α-process for MCM-41 loaded with naproxen. 54

LIST OF ABREVIATIONS:

α- symmetry broadening the spectrum

ATR-FTIR- Infrared Spectroscopy by Attenuated Total Reflectance

$\beta-$ asymmetric broadening spectrum

B- broadening the spectrum parameter, characteristic of the material

BCS- Biopharmaceutics Classification System

BET- Brunauer–Emmett–Teller

BJH- Barrett-Joyner-Halenda

CP- Cross Polarization

$\Delta C_p -$ Change in heat capacity

De- dielectric strength

DFT- Density Functional Theory

$\Delta H_c -$ Change in Enthalpy of Crystallization

$\Delta H_m -$ Change in Enthalpy of Fusion

D_p - Pore diameter

DRS - Dielectric Relaxation Scanning

DSC - Different Scanning Calorimetry

ε_∞ - optical dielectric constant (real permittivity at infinite frequency)

f_{max}- Maximum frequency

G- Shear modulus

HN-Havriliak Negami

HO-Si-OH- geminal silanol groups

HO-Si-Si-O-OH- vicinal silanol groups

IR-Infrared Spectroscopy

J_{growth} – rate of crystal growth

$J_{nucleation}$ – nucleation rate

MAS- Magical Angle Spinning

MCM-41- Mobil Composition of Matter No. 41

MCM-41_Func- Mobil Composition of Matter No. 41 functionalized loaded with naproxen

MCM-41_Func_Naproxen- Mobil Composition of Matter No. 41 functionalized loaded with naproxen

MCM-41_Naproxen- Mobil Composition of Matter No. 41 loaded with naproxen

NMR- Nuclear magnetic resonance

Q^2- geminal silanol groups

Q^3- vicinal or isolated silanol groups

Q^4- surface siloxanes

Q^n- Attributed nomenclature to the different silanol groups on the silica surface

S- Specific Surface

Si-O-Si - surface siloxanes

τ_0- characteristic relaxation time

T_c- Crystallization Temperature

T_g- Glass Transition Temperature

$T_{g(endset)}$- Glass Transition Temperature endset

$T_{g(midpoint)}$- Glass Transition Temperature midpoint

$T_{g(onset)}$- Glass Transition Temperature onset

$T_{g,t=100\ s}$- Dielectric Glass Transition at a Relaxation Time of 100 s

T_m- Melting Temperature

T_o- Vogel Temperature

υ – infrared stretching vibration

υ_{as}–– asymmetric infrared stretching vibration

υ_s– symmetric infrared stretching vibrations

VFTH- Vogel-Fulcher-Tamman-Hesse

V_p- Total Pore volume

ω- angular frequency

α- alpha process

τ – torsion vibrations infrared

$\varepsilon'(\omega)$- Real part of the complex permittivity

$\varepsilon''(\omega)$-Imaginary part of the complex permittivity

1 Introduction

1.1 Motivation

For a long time now, drug solubility has been a topic of interest for research and development in the pharmaceutical industry. Low water solubility is a common characteristic of many pharmaceutical drugs, therefore requiring an intake of higher dosage, so the essential levels for treatment are reached in the blood.[1] with a consequent negative impact in the environment[2] and on the cost of marketed drugs.

The process of drug development is complex and requires many phases and steps. World researches to have success in their investigation must make a highly specific drug, with high affinity to its biological targets to reduce the probability of undesired side effects. This is the stage where attempts are made to improve drug solubility, not compromising pharmacokinetics and pharmacodynamics. There are many approaches been taken in consideration to improve drug's solubility, some examples are: amorphization, micronization, crystal modification, etc.[3]

This assignment focus in the amorphization of a poor water soluble crystalline drug (naproxen). The strategy is, by incorporating it in two silica (MCM-41and functionalized MCM-41), its dissolution rate and bioavailability will improve.

1.2 Naproxen

(S)-(+)-6-Methoxy-α-methyl-2-naphthaleneacetic acid, more commonly known as naproxen is a pharmaceutical drug that acts as an anti-inflammatory nonsteroidal with analgesic and antipyretic properties.[4,5]

Naproxen is an enantiomeric drug, being the enantiomer S, the one used for health treatments and the enantiomer R is toxic. The structure of the drug is formed by two aromatic rings and a carboxylic acid having a pKa of 4.15.[5] Naproxen is most commonly used for the treatment of rheumatic diseases and acute painful procedures. Due to some of its characteristics, as low solubility and high permeability naproxen belongs to the second class of the biopharmaceutical classification system.

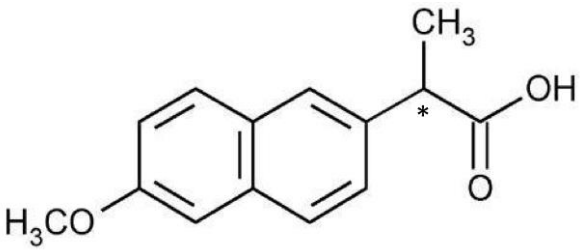

Figure 1. Representation of naproxen molecular structure. * indication of the chiral centre.

1.3 Bioavailability and Biopharmaceutics Classification System (BCS)

Bioavailability quantifies the rate in which the drug is absorbed and the fraction of the unchanged drug that was taken in that will reach the systemic circulation.[6] Characteristics as permeability and solubility are extremely important in the determination of drug's oral bioavailability. For many pharmaceutical drugs, solubility is a challenge, as it is so difficult to develop proper formulation for oral administration.[7]

Dissolution is extremely important when it comes to the rate-determining step in the pharmaceutical drug absorption. Bioavailability in this case is contrariwise related to the distribution of particle size when pharmaceutical drugs present properties like, low solubility, and dissolution rate.[8] It is intended that by increasing solubility, bioavailability will increase too.[9] So, many tactics are being developed with the drive to enhance the solubility, dissolution rate and oral bioavailability of poorly water drugs.[10]

The purpose of the Biopharmaceutics Classification System was to gather information on in-vitro dissolution and in-vivo absorption, by associating this information different drugs could be classified.[11]

The BCS is a mathematical model that measures solubility and permeability under exact conditions.[11] Characteristics as aqueous solubility relating do dose and intestinal permeability in combination with dissolution properties are the base of classification of drugs into four classes.[11] The classes are the following: class I contains all the drugs that have high solubility and permeability due to strategy. In classes III and IV the drug´s bioavailability is conditioned by its permeability. Drugs in class II, the case of naproxen (under study), are poorly soluble. Naproxen's solubility is 1.26 g/L (25 ºC)[4], which is very low, so, the aim is to improve its solubility in the aqueous medium.

Table 1. Representation of the Biopharmaceutics Classification System. [11]

Class	Solubility	Permeability
I	High	High
II	Low	High
III	High	Low
IV	Low	Low

The system can classify the drug in its early stages, which is an important factor, as it can influence the decision to continue studying the drug or not. The system has gained more and more importance nowadays.[11]

1.4 Crystals and Amorphous Materials

Solid matter can be classified as crystalline, amorphous or a mixture of the two. In crystalline solids, atoms are arranged in a long-range order in a three-dimensional space. On the other hand, amorphous solids show no organization, it only exists local order of atoms, due to the interactions between them. Amorphous materials are defined as non-crystalline, because atoms do not show an organized pattern[12] (figure 2).

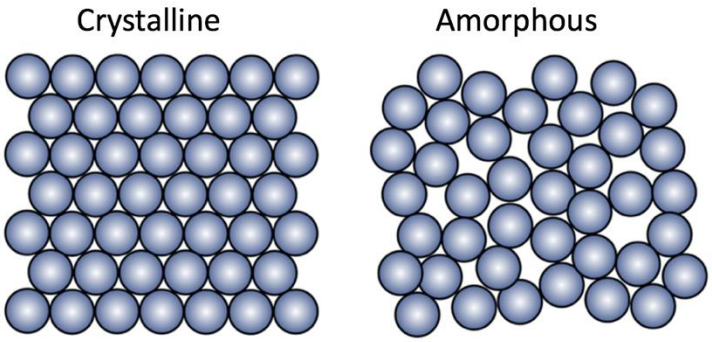

Figure 2. Amorphous solids vs Crystalline solids.

Such characteristics, as disorder, give amorphous properties as a higher Gibbs free energy, a faster solubility and dissolution rate, resulting in an increase in therapeutic activity, by comparing these two types of solids. However, a higher entropy, enthalpy and Gibbs free energy make amorphous solids less stable and act as a driving force to the occurrence of crystallization.[13]

Crystallization is a known first-order transition (it has latent heat associated), so the temperature will not change until the transition is completed.[14] As an exothermic reaction, passing to a more stable state, crystallization is a combination of two steps. Nucleation and crystal growth.[15] For this transition to happen, a nucleus is required for the crystal to grow, if nucleus is present than the material during cooling becomes a glass. The nucleus is either homogeneous or heterogeneous. If the nucleus is homogeneous, the crystal will form spontaneously during melting, if it is heterogeneous forms a pre-existing surface of an impurity.[15]

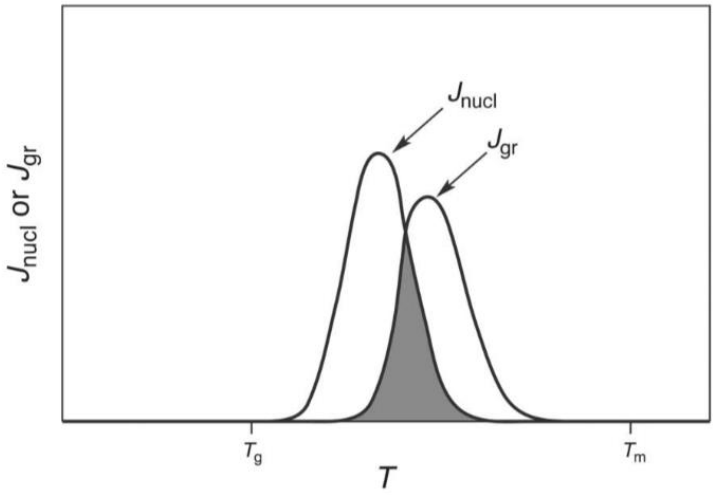

Figure 3. Demonstration of nucleation rate, $J_{nucleation}$, and rate of crystal growth, J_{growth}, in respect to temperature. T_g is the glass-transition temperature, T_m is the melting temperature, units are arbitrary for rate. The area where the curves overlap, in grey, is the temperature range where nucleation and growth happen.[15]

1.5 Phase Transitions

Phase transitions happen when a material changes from a state (ex. solid, liquid or gas) to a different state. This happens at a combination of certain conditions, temperature and pressure. Examples of very familiar transitions are: condensation, vaporization… However there are those less known as: solid-solid, etc. As it can be seen, there are many different types of phase transitions, each with their own specific characteristics and they can be classified agreeing to their thermodynamic properties.[16]

In first-order phase transitions, the energy that is supplied, turns into latent heat, this occurs at a stationary temperature, until the transition is concluded. The difference in enthalpy, volume, entropy is finite at this fixed, specific temperature. The first derivative of these measures with respect to temperature is discontinuous. Examples of first-order transitions are melting, boiling and crystallization.[16]

In second-order transitions regarding temperature, the first derivative is continuous and the second is discontinuous. The same properties as given above, enthalpy, entropy and volume do not change.[16]

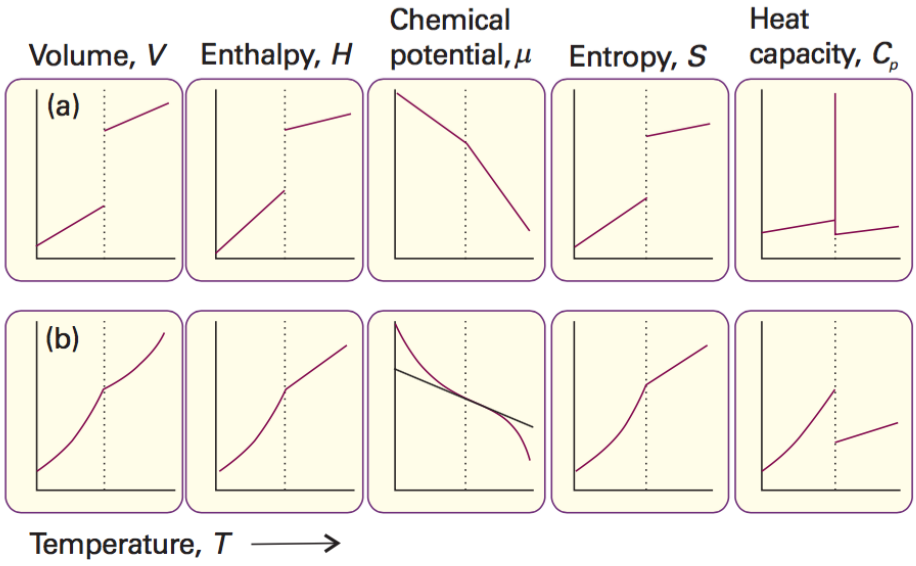

Figure 4. Thermodynamic properties changes in a) first order phase transitions and b) second order phase transitions[16]

1.5.1 Melting

Melting is a first order transition, and when it occurs, the substance becomes more disorder, in a liquid-like form.[14] Many things are happening to a material while its melting, as: disorder increases (endothermic process having a melting enthalpy ΔH_m associated with it)[14]. The volume and heat capacity always changes. The heat capacity is defined as the quantity of heat that is required to raise the temperature of an identified system by one degree.[17]

The process of melting can only take place if the substance is crystalline. The theory says that melting occurs by an instability created as temperature increase, in the crystal lattice structure. [14]

1.5.2 Glass Transitions

Having a continuous first derivative and a discontinuous second derivative, glass transition is classified as a pseudo-second-order transition as it does not happen between two states of thermodynamic equilibrium[18], so it's not considered a true phase transition because there aren't discontinuous changes in the physical properties.[19] This so-called transition, can only happen in amorphous material, as it has no latent heat associated and where enthalpy, volume and entropy change continuously.[19]

The glass transition takes place, when a liquid is being cooled below the melting point, fast enough that it can dodge crystallization to enter in a supercooled state. As the system gets cooler and cooler, undergoes solidification due to the increase of viscosity it's molecular mobility slows down[19] to turn into a glassy substance. This transition has a ΔCp (heat capacity) associated, and it occurs over a range of temperatures, ($T_{g,onset}$, $T_{g,midpoint}$ and $T_{g,endset}$) see figure 5. This characteristic behavior of the glassy material preserves the liquid-like characteristics from its originating liquid.[19,20]

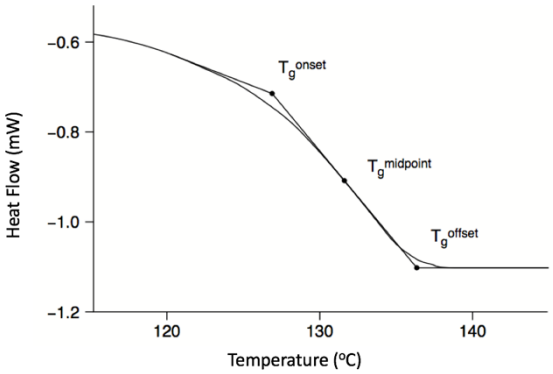

Figure 5. Representation of T_g from a DSC scan, idientification of onset, midpoint and offset or endset.

The characteristics of the glass are dependent on the rate at which is formed. So, it doesn't fall out of the liquid-like equilibrium, a slower cooling treatment is applied, giving enough time for configurational arrangement at each temperature, consequently originating a glass transition at lower temperatures.[19] (See figure 6)

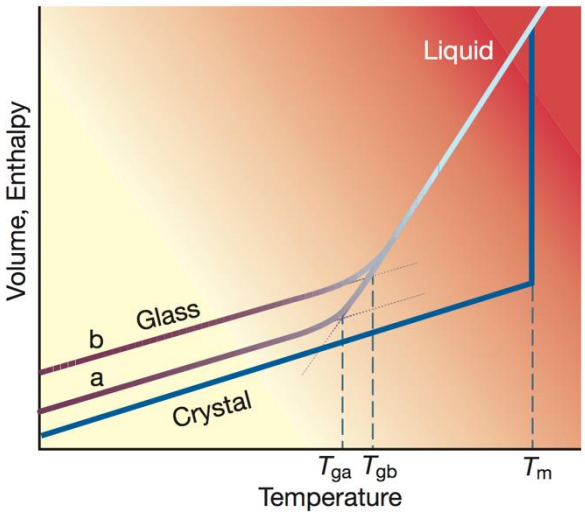

Figure 6. Representation of temperature dependence on enthalpy and volume. T_{ga} is the glass transition temperature formed from a slow cooling rate and T_{gb} from a faster. T_m is the melting temperature.[19]

This state (glassy), is out of equilibrium, therefore it has a spontaneous tendency to convert into a more thermodynamically stable form, consequently recrystallization can occur, above or below T_g, making it interesting and fundamental to study strategies to avoid this trend.[19]

1.6 Silica MCM-41

The MCM-41 (Mobil Composition of Matter No. 41) is a favourable member of the mesoporous silicate family and of the aluminosilicate materials.[21,22] The MCM-41 has a regular pore system, consisting of hexagonal display and shaped pores, as well their highly specific pore volume (up to 1.3 ml g^{-1})[21] and surface are (up to 1500 m^2 g^{-1})[21], make them so promising for many uses, as drug carriers. [23] When silica is used in such a way, the drug is loaded and then locally released in a controlled way, providing a precise delivery to the target site. [22]

Modifying (functionalizing) the silica pore inner walls, can have a crucial role, as by changing the surface it can alter the binding strength, consequently having an impact on the release rate.[24–26] These aspects keep increasing the interest of researchers and industry in these materials.

The term known as controlled release is given to an experiment that studies the performance or delivery of a compound in response to time or stimuli.[8] These experiments are normally tested under conditions that will try to simulate body features, so, that they can mimic the period of release and how it is released in the bloodstream.[8]

1.7 Techniques

1.7.1 Attenuated Total Reflectance Fourier Transform Infrared Spectroscopy (ATR-FTIR)

Infrared (IR) spectroscopy is a very well-known and extremely reliable fingerprinting technique, as it can identify, characterize and quantify many substances; solids, liquids and gases. The spectrometers, use infrared radiation to analyse the samples by the transmitting directly through them, no matter the type. The determination of the spectral features intensity depends on the thickness of the sample, so, therefore, a precautious sample preparation is mandatory to acquire good readings.[27]

The technique of attenuated total reflectance (ATR), is a modernization of analyses for liquid and solid samples. In the traditional IR, solid samples preparation involves crushing the substance to a fine powder and dispersing it into a matrix. The compound being analysed is either mixed with a liquid or a solid, potassium bromine (KBr) is probably the most widely used. The mixture is then pressed, turning into a clear glassy disk, ready to be analysed in the spectrometers. Liquid samples are more commonly analysed as thin films in cells, the cell consists of two infrared transparent disks. Sample preparations are easier for liquid samples than solid ones, however both type of samples cannot be used again.[27]

The attenuated total reflection accessory works by measuring the variations that happen when the beam encounters the sample. This beam is directed onto an optically dense crystal with a high refractive index for a specific angle, this internal reflectance will create an evanescent wave that will reach beyond the surface of the crystal into the sample, and it will seat on the surface of the crystal. This wave projects only a few microns beyond the crystal wall into the sample, therefore there must be good contact between both. The evanescent wave will suffer changes (altered or attenuated) in the regions of the spectrum where the sample absorbs energy. This attenuated or altered energy return to the beam, in the opposite end of the crystal, passing through the detector, where the system generates an infrared spectrum.[27]

So, to have good results with this accessory, there are two important aspects to take in account. The sample being analysed must be in direct contact with the crystal while the evanescent wave only reaches a very small distance of 0.5 μ - 5 μ[27] past the crystal. The second aspect is that the refractive index of the crystal must be greater than the one from the sample, otherwise internal reflectance does not happen, so instead of being transmitted the light is reflected in the crystal. Usually the ATR crystals have a refractive index between 2.38 and 4.01 at 2000 cm^{-1}. [27]

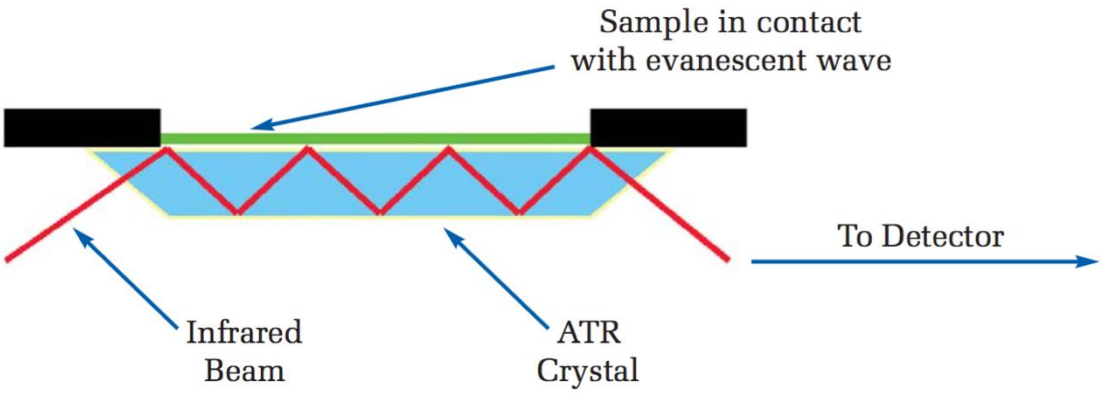

Figure 7. Scheme of a multiple reflection in ATR-FTIR.[27]

1.7.2 Thermogravimetric Analysis (TGA)

The technique of thermogravimetric analysis consists in the examining of a mass sample over time or temperature, the substance is exposed to a controlled atmosphere and temperature program. This means, the TGA controls the weight of the sample being analysed as it is cooled or heated. Thermogravimetric analysis is very used to characterize a variety of materials in various sectors as environment, pharmaceutical, petrochemical and food industries.[28]

The sample goes into a pan supported by a precision balance. The pan will stay in a furnace and depending on the type of experiment it will be cooled or heated. The weight of the pan (sample) is being monitored all the time. The control of the atmosphere is done by using sample purge gas.[28]

Through this technique, it is possible to quantify the amount of mass that remained and the amount of mass that degraded. The loading percentage of the matrix is calculated with the given equation:

$$\%\ Loading = \frac{Mass\ of\ Naproxen}{Mass\ of\ Naproxen + Mass\ of\ Silica} X\ 100 \qquad \textbf{Eq.1}$$

1.7.3 Scanning Electron Microscopy (SEM)

A scanning electron microscope is uses a beam of high-energy electrons, that will emit a variety of signals when encountering the surface of the solid material being analysed. The interactions that are created between the electrons and the surface reveal information about the solid sample like: the texture, the orientation about the materials and its crystalline structure. When the data is being gathered, most of the time, is obtained over a chosen area to generate a 2-dimentional image that displays the properties all the characteristics mentioned above.[29,30]

1.7.4 Transmission Electron Microscopy (TEM)

TEM is a technique where a beam of electrons is transmitted through an extremely thin sample, the thickness of the sample is about 100 nm. The interactions between the sample and beam create an image. This image will then be magnified onto a fluorescent screen or others. This type of microscope can capture extremely small detail as a single column of atoms. TEM is an extremely useful analytical method in chemistry, biology and physics. An example it has some applications in cancer studies.[31]

1.7.5 Differential Scanning Calorimetry (DSC)

Differential Scanning Calorimetry is a technique which studies thermal transitions, as solid-solid, solid-liquid transitions, among others. It measures a chemical or physical change, when energy is transferred as heat to or from the sample being studied. During these analyses, it is possible to understand what is happening to the material, even if there are no visual changes. This is done, by comparing the behaviour of the sample with a reference material, which does not undergo any physical changes during the time of the analysis. [14]

In the apparatus, there are two pans that are isolated from the surroundings. One of the pans is the reference pan, that is empty, and the other contains the sample being analysed. There is one heater underneath each pan, to regulate the temperature and a sensor that will indicate it. So, the heating or cooling rate is constant for both pans, the apparatus adjusts both heaters. The heaters are programed to heat or cool both pans at a constant rate ($\Delta T/\Delta t$), and at the same rate as each other, so the rate in temperature

change is the same for the reference pan and the sample pan. The heat flow, that is the rate of thermal energy ($\Delta Q/\Delta t$) being supplied to both pans does differ, because the heat capacity is different since one pan is empty (reference) and the other pan contains the sample being examined. This difference in the heat flow between both pans is plotted against temperature.[17,32]

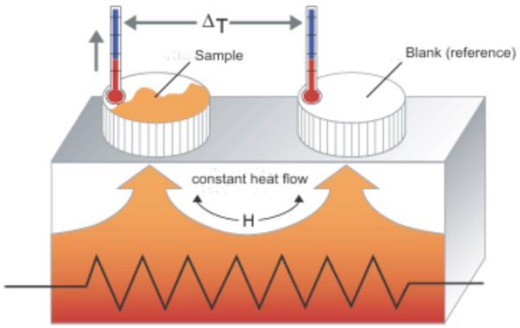

Figure 8. Diagram representation of the heat-flux of differential scanning calorimetry.[32]

As it was previously mentioned, the heating rate ($\Delta T/\Delta t$) is set, and the heat flow ($\Delta Q/\Delta t$) is measured as endothermic (melting) or exothermic (crystallization) peak (see figure 9). The values of enthalpies associated with melting and crystallization are calculated by integrating the area of respective peaks. Glass transition, on the other hand, is identified as a step in the thermogram. Through the slope of the glass transition step, the change in the heat capacity (ΔC_p) can also be calculated by dividing the heat flow by the heating rate (see equation 2).[17,33]

$$\frac{(\Delta Q/\Delta t)}{(\Delta T/\Delta t)} = \frac{\Delta Q}{\Delta T} = \Delta Cp \ (J\ ^oC^{-1}) \qquad \textbf{Eq. 2}$$

The calorimetric apparatus divides the heat capacity by the mass of the sample, providing the specific heat capacity.

$$\frac{\Delta Cp}{m} = \Delta Cp \ (J\ ^oC^{-1}\ g^{-1}) \qquad \textbf{Eq. 3}$$

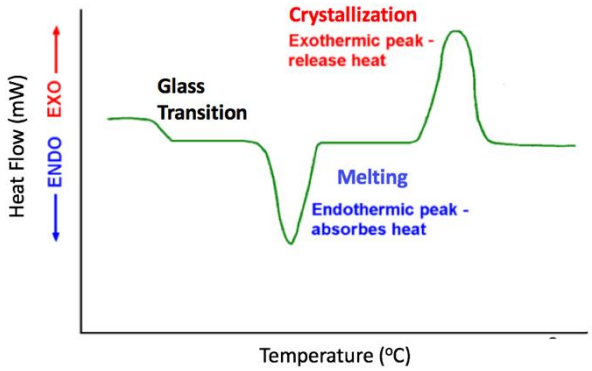

Figure 9. Differential Scanning Calorimetry profile with exothermic and endothermic heat flow plotted versus temperature.[33]

1.7.6 Nuclear Magnetic Resonance (NMR)

SS-NMR, or solid-state nuclear magnetic resonance is a technique that delivers information about the structure of molecules to an atomic level, and nowadays it is applicable in almost all scientific fields. To obtain in a detailed information as solution-nuclear magnetic resonance, additional techniques are required for ss-NMR as magic-angle spinning (MAS) and cross-polarization (CP), between others.[34]

The MAS involves the rotation of the sample 54.74 º with respect to the magnetic field, so that anisotropic dipolar interactions are diminished. For this technique to be effective, the spinning must happen at the same or higher rate than the dipolar linewidth. The CP, cross-polarization technique implicates the displacement of polarization from some more abundant nuclei (as proton) to some lesser common ones (as carbon), with the purpose of enhancing the reason signal/noise.[35]

^{29}Si ss-NMR coupled with cross-polarization and magic-angle spinning is a very consistent technique to quantify the nature of solid silica matrixes, specially of amorphous silica.[36] Through this type of spectrum, it is possible to distinguish different silanol groups; geminal (Q^2) with a peak at -92 ppm, vicinal or isolated (Q^3) at -101 ppm and surface siloxanes (Q^4) at -110 ppm.[36–38]

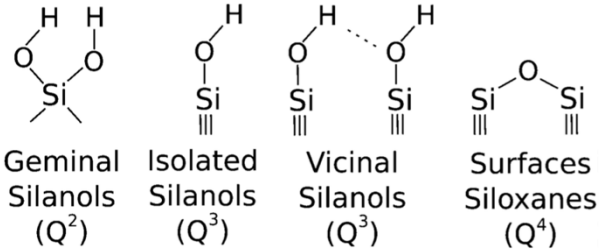

Figure 10. Attributed Q^n nomenclature to the different silanol groups on the silica surface.[36]

In the silicas being studied, the expected results from the analyses of the modified one, a reduction in Q^2 and Q^3 peaks and an increase in Q^4 intensity.

The ^{13}C NMR aids by giving supplementary information on the alkyl groups bonded on the surface of the modified matrix, indicating a successful functionalization.[34]

1.7.7 Dielectric Relaxation Spectroscopy (DRS)

From the dielectric relaxation technique, it can be studied the dipole relaxation caused by the reorientation motions of molecular dipoles and the originating electrical conduction due to the translational motion of electrons and ions, in a range of frequencies of 10^{-6} to 10^{12} Hz.[39]

When a non-conductor sample, that must contain permanent dipoles, is under an oscillating electric field a net polarization is caused.[39,40] Atoms combine by sharing one or more electrons to form a molecule. As this combination is being formed, the rearrangement may origin an unequal dispersion of electrons, forming a so called dipolar moment. This dipolar moments are not organized in precise order, instead they have a random distribution, but when they are submitted to an electric field, a re-orientation of the dipoles occurs so they align with the field, therefore causing polarization.[39,40] By reversing the electric field, once more the dipole rearranges itself to stand the alignment, while reorientation happens, energy is lost.[39,40]

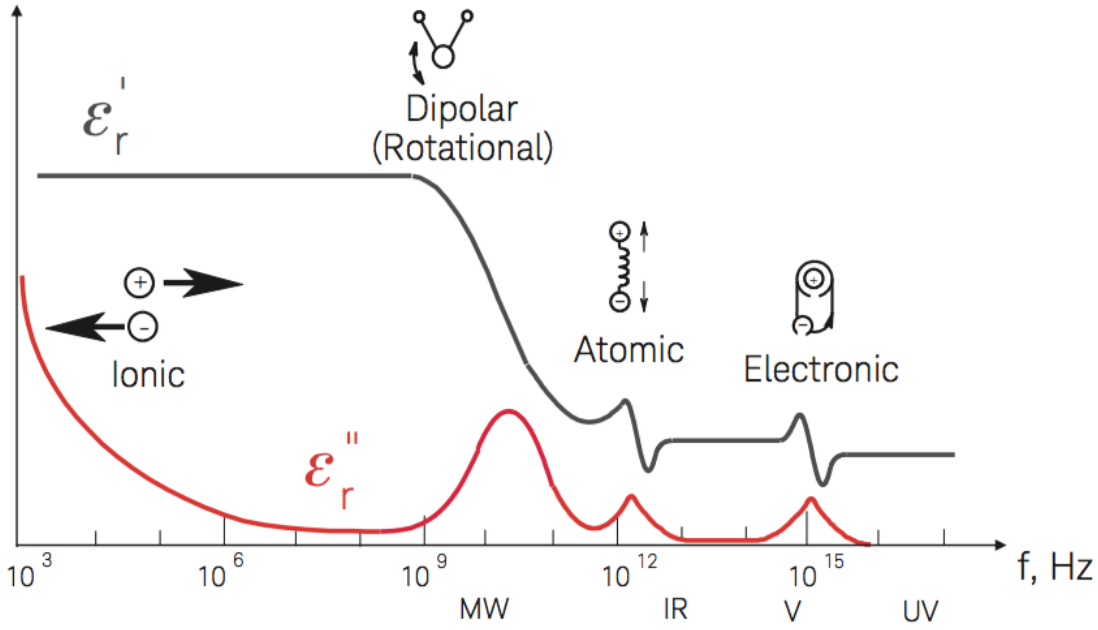

Figure 11. Frequency response of the dielectric mechanisms.[38]

Permittivity (ε^*) is the measure of the quantity of charge needed to generate an electric field at a specific medium. The amount of energy that is gathered in the dielectric material from the external electric field is known as the real part of permittivity (ε').[40] The energy being lost from the dielectric substance is the imaginary part of the permittivity (ε''). The ε'' is always greater than zero[40] and the greater it is, the more energy is being dissipated (lost), therefore leaving less energy available to the dipole re-orientate. This is linked to the intrinsic loss of the system, and it is recognized as the dielectric loss. [39]

The complex dielectric permittivity function is given by:

$$\varepsilon^*(\omega) = \varepsilon'(\omega) - i\varepsilon''(\omega) \qquad \textbf{Eq.4}$$

Where:

- ω is the angular frequency of the applied electric flied
- ε' (ω): is the real part of complex permittivity, quantifying the polarization stored by the system, given by the ratio between the sample capacitance C, and the capacitance when the measuring cell is vacuum filled, C_0, so $\varepsilon' = C/C_0$
- ε'' (ω): is the imaginary part, or dielectric loss being the dissipated energy, and is quantified by the resistance, R, reciprocal as $\varepsilon'' = 1/(RC_o\omega)$

When the frequency of the applied field is low, dipoles have time to align with the electric field. However, as frequency increases, dipoles become unable to follow the oscillating filed. Increasing the frequency, increases the imaginary part, and a maximum value will be achieved at f_{max}. This maximum peak of ε'' is related to the characteristic relaxation time. The relaxation time (τ), is the time needed for the displaced system aligned with the electric field to restore its random distribution of equilibrium by an amount of 1/*e* (where *e* is the Neper number), after the electric field is removed.[39,41]

The higher the temperature at which each spectrum is collected, the more mobile dipoles are and therefore, higher f_{max}. This maximum ε''-peak frequency is related to the characteristic molecular relaxation time, τ, measuring dipoles mobility in a material.[40,41] Therefore, the relaxation time is estimated from the frequency location of the maximum dielectric loss peak through the following equation[39]:

$$\tau_{max} = \frac{1}{2}(2 * \pi * f\max) \qquad \textbf{Eq. 5}$$

In conventional glass, former systems, i.e., materials that avoid crystallization, entering in the supercooled state and vitrifying upon further cooling, the molecular mobility can be probed by dielectric spectroscopy near above and below the glass transition. In this dynamical range, the characteristic relaxation times fit within the frequency range of routine dielectric spectroscopy (10^{-2} to 10^{6} Hz). Since amorphous materials are dynamically heterogeneous, even when only one dipole type is present, regions from high mobile and low ordered to low mobile and highly ordered and combinations in between coexist, a distribution of relaxation times instead of a single τ, is needed to adequately describe the system. Experimentally, spectra are collected over a frequency window and covering a temperature range, but each one is acquired at a constant temperature, at which different molecular motions associated with distinct relaxation processes can be active. Therefore, to proper simulate each spectrum, a sum of relaxation processes may be needed. The most popular, although empirical, model function used to analyse the isothermal dielectric spectrum is the Havriliak-Negami (HN)[39]. When there are several relaxation processes, a sum of HN functions is applied.

$$\varepsilon * = \varepsilon_\infty + \sum_{j=0}^{n} \frac{\Delta\varepsilon_j}{(1+/(i\omega\tau_0)^{\alpha j})^{\beta j}} \qquad \textbf{Eq.6}$$

Where:

- ε_∞ : optical dielectric constant (real permittivity at infinite frequency)
- $\Delta\varepsilon$: dielectric strength
- τ_0: characteristic relaxation time
- ω: angular frequency
- α and β: describe the symmetry and asymmetry broadening the spectrum, within a range $0 < \alpha < 1$ and $0 < \alpha.\beta < 1$.[42]

The different relaxation processes active simultaneous at a definite temperature can exhibit distinct temperature dependencies. While very localized mobility is temperature activated – Arrenhian (linear) temperature dependence, some cooperative processes, as the glass transition, have a non-linear dependence on temperature, following a non-Arrhenius law. This nonlinear dependence is described by the Vogel-Fulcher-Tamman-Hesse (VFTH) equation, that is shown below[39]:

$$\tau(\mathrm{T}) = \tau_\infty * e^{(\frac{B}{T-T_O})} \qquad \textbf{Eq.7}$$

where:

- τ_∞: relaxation time at a high temperature limit
- B: parameter specific to each material
- T_o: Vogel temperature

To obtain the glass transition temperature, and since is not a true transition in the usual thermodynamic sense, it is required some criteria to identified it, as the temperature at which the relaxation time,τ becomes 100 s. The reason for this value, derives from the Maxwell relation.[39]

$$\eta\,(Pas^{-1}) = \tau_{max}\,(s) * G(Pa) \qquad \textbf{Eq. 8}$$

Where:

- τ_{max}: relaxation time to 100 s
- η: viscosity of a solid
- G: the shear stress

A η (viscosity) of 10^{12} Pa and a G (shear stress) of 10^{10} Pa characterises a solid and, therefore, from Eq. 8, a relaxation time of 100 s is obtained.

The substitution of τ=100 s it in the VFTH equation, allows to estimate the so-called dielectric T_g. [39]

1.7.8 Ultraviolet Spectroscopy (UV-Vis)

When electrons are excited from a lower level into a higher level, visible and ultraviolet radiation are absorbed or transmitted. In both, visible and ultraviolet radiation the electron is excited from a full orbital (low energy) to an empty, anti-bonding orbital (high energy), becoming excited. Each wavelength has an energy coupled with it, so if the precise amount of energy is supplied to make the electronic transition, then the wavelength will be absorbed. The bigger the difference between the energy levels, more energy is required to move the electron. So, the higher the energy, the higher frequency and the shorter the wavelength will be.[43]

This type of spectroscopy allows the determination of sample's concentration and rate equations, dissolution rates and the study of reaction rates, as many others. UV-spectroscopy is widely used in quantitative analyses for all the molecules that absorb in ultraviolet and visible electromagnetic radiation. [43,44]

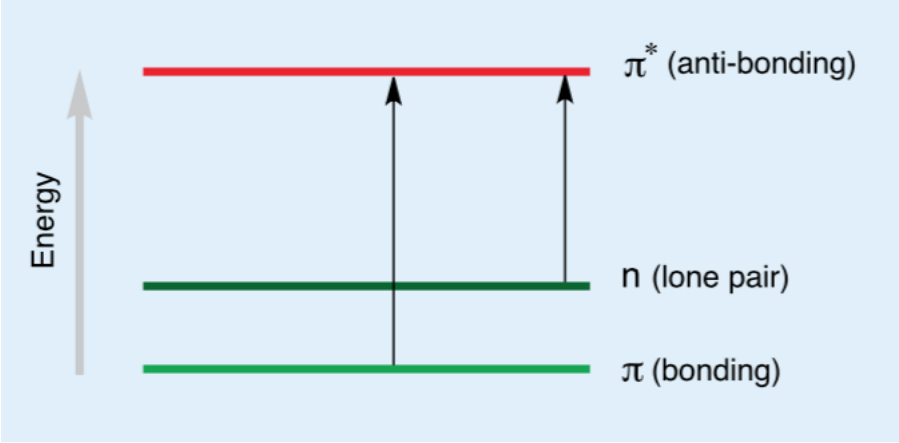

Figure 12. Representation of electronic transitions that results from light absorption.[42]

2 Methods and Materials

2.1 Synthesis of Mesoporous MCM-41

2.41 g of n-hexadecyltrimethylammonium bromide (C_{16} TMABr) was weigh and dissolved in 10.46 ml of aqueous ammonia (25 wt. %, 0.14 mol) and in 120 ml of deionized water, to obtain a concentration of 0.055 mol L^{-1}. The solution was under stirring for about one hour, until there was no foam left. 10 g of TEOS (tetraethoxysilane, 0.05 mol) drop by drop was added to the surfactant solution, still under stirring, it stayed like that for one hour. The white precipitate formed was washed with 100 mL of deionized water and removed by filtration under vacuum. The sample was left to dry at 90 ºC for nineteen hours. It was then heated to 550 ºC at 1 ºC/min for nine hours, to remove the template. [21]

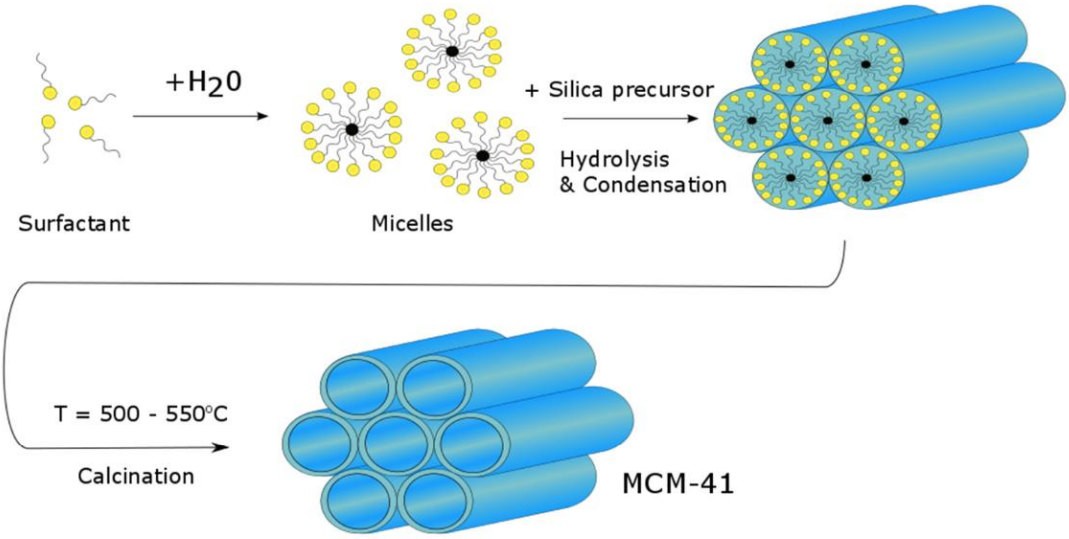

Figure 13. Representation scheme of the MCM-41 synthesis.[22]

2.2 Functionalization of the Mesoporous Silica MCM-41

0.504 g of the MCM-41 were weigh in to a small flask and left in an incubator oven at 100 ºC all night. 150 ml of dry toluene were previously prepared by using molecular sieves (activated by being heated up to 300 ºC for one hour) and sodium lumps, which create bubbles when there is still water present. The sample of MCM-41 was removed from the incubator oven to a three-neck round bottom flask. 2.5 ml of methyltrimethoxysilane and 150 ml of dried toluene were added in to the three-neck round bottom flask. One of the necks of the three three-neck round bottom flask was connected to a nitrogen hose, the second one was connected to a condenser and the third neck was closed with a glass stopper. The solution was left under stirring in an oil bath at the temperature of 80 ºC for a period of five hours. The solution was then filtered and washed with 50 ml of dry toluene and ethanol. Finally, it was left to dry overnight in an oven at the temperature of 100 ºC.[24,45]

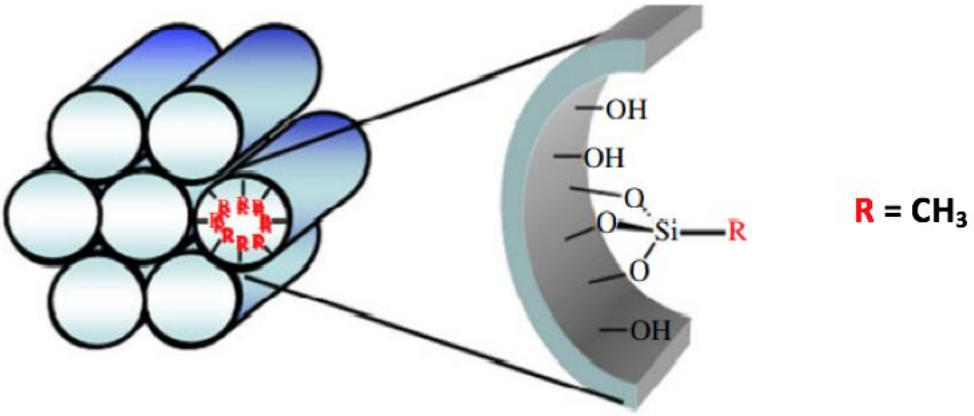

Figure 14. Representation of MCM-41 functionalization. Adapted[43]

2.3 Textural analyses of MCM-41 and MCM-41 Functionalized by Nitrogen Absorption Analysis

Both matrixes were characterized and analyzed by nitrogen porosometry in the Laboratório de Análises/Requimte of the Chemistry Department of NOVA University of Lisbon. Nitrogen absorption isotherms were measured at -196 ºC. Before the analyses the sample was outgassed at 200 ºC under vacuum for 1 hour. The following textural properties were obtained:

Table 2. Textural properties of MCM-41 and MCM-41 functionalized.

Sample	S_{BET}[a]/ $m^2\ g^{-1}$	Vp[b]/ $cm^3\ g^{-1}$	Dp[c]/nm
MCM 41	986.1685	0.74117	3.0
MCM 41_Func	944.7177	0.70630	2.9

a) The specific surface area (S) was determined from linear portion of the Brunauer-Emmett-Teller (BET) plots
b) The specific total pore volume (Vp) by density Functional Theory (DFT) method
c) Pore size distribution (Dp) was determined by the Barret-Joyner-Halenda (BJH desorption)

2.4 Drug Loading

To incorporate naproxen in the silica, it was first necessary to remove water and impurities that could exist in both silica. 159 mg of MCM-41 and 152 mg of MCM-41-Func were weighted into glass cells and were submitted to vacuum, 5 mbar and emerged in a paraffin bath to be heated for seven hours (temperatures between 140 ºC up to 170 ºC). The samples were then left to cool down for 30 minutes before inclusion.

Figure 15. Assembly line for drug loading process.

To estimate the amount of naproxen for inclusion, the filling percentage was calculated by using silica's pore volume and naproxen's density in the following equation:

$$\%\ Filling = \frac{\frac{Mnaproxen\ (g)}{\rho naproxen\ (\frac{g}{cm^3})}}{pore\ volume\left(\frac{cm^3}{g}\right) * Msilica\ (g)} * 100 \qquad \textbf{Eq. 9}$$

The mass was calculated to a filling of 80 and 75 % for MCM-41 and MCM-41_Func respectively, so, there wouldn't be any naproxen outside pores. The masses of naproxen were dissolved in 1 ml of chloroform, and with the glass cells still under vacuum, they were added to each sample of silica. The resulting composite was left to dry for forty-eight hours at 50 ºC, under stirring with two magnetic bars, until all the chloroform had evaporated. After the two days, the mixtures were removed from the glass cells, and stored in eppendorfs.

2.5 Scanning Electron Microscopy (SEM)

The samples were analysed by Microlab, Electron Microscopy Laboratory in Instituto Superior Técnico de Lisboa. The morphology of the sample was observed by using a high-resolution scanning electron microscope Hitachi-S-2400/Bruker.

2.6 Transmittance Electron Microscopy (TEM)

The samples were analysed by Microlab, Electron Microscopy Laboratory in Instituto Superior Técnico de Lisboa. The morphology was observed by using a high-resolution electron microscope Hitachi H8100/ThermoNoran System SIX.

2.7 Thermogravimetric Analyses (TGA)

The TGA analyses was used to evaluate the percentage of loading of naproxen in each silica. These analyses were realized by Centro de Investigação de Materiais (CENIMAT). About ~5 mg from each sample were placed in an open aluminium pan. The thermogravimetric measurements were carried out from room temperature to 550 ºC in the device Simultaneous Thermal Analyser (TGA-DSC – STA 449 F3 Jupiter) from Netzsch, the heating rate was of 50 ºC.min^{-1}. The sample was under pure nitrogen atmosphere; the sample purge flow rate was of 60 ml.min^{-1}. The temperature readings

were calibrated using Curie points of nickel standard, while the mass reading was calibrated using a balance tare weights from TA.

2.8 Attenuated Total Reflectance Fourier Transform Infrared Spectroscopy (ATR-FTIR)

The device used was a PerkinElmer Two IR Spectrometer. A small quantity of the samples, each at a time was placed onto the diamond crystal area and the pressure arm of the device was positioned over the sample. Pressure was applied pushing the sample onto the diamond surface to achieve the best resolution possible. The spectra were obtained by Spectrum 10 software, also from PerkinElmer. The samples were analyzed in the 400 to 4000 cm^{-1} spectrum range with 16 scans of resolution.

2.9 Nuclear Magnetic Resonance (NMR)

Solid state ^{13}C MAS and ^{29}Si MAS NMR spectra were acquired in a 7 T (300 MHz) AVANCE III Bruker spectrometer operating respectively at 75 MHz (^{13}C) and 60 MHz (^{29}Si), equipped with a BBO probehead. The samples were spun at the magic angle at a frequency of 10 kHz in 4 mm-diameter rotors at room temperature. The ^{13}C MAS NMR experiments were acquired with proton cross polarization (CPMAS) with a contact time of 1.2 ms, and a recycle delay of 2.0 s.

The ^{29}Si MAS NMR spectra were obtained using a single pulse sequence with a 90° pulse of 4.5 μs at a power of 40 W, and a relaxation delay of 10.0 s.

2.10 Different Scanning Calorimetry (DSC)

All the samples were analysed by DSC: native naproxen, both empty matrixes, MCM-41 and MCM-41_Func and the respective composites. In a precision balance (Sartorius Research M-power), an aluminium pan and lid (TA Tzero Hermertic Lid and Tzero Pan) were weighed for each sample. The average of the mass samples should be about 2-5 mg. All pans are sealed before the analysis. The masses of pans, and samples were noted for future calculus.

Before the analysis in the DSC, the pans are perforated with a pin to ease water/ solvent evaporation during heating processes, so bursting due to over pressure is avoided. The pan is then placed inside the DSC Q2000, with a RCS 90, on top of a temperature sensor, next to empty closed pan, that is used as reference. The temperature variation ramps

(thermal procedure) and the respective masses (pan, reference pan and sample) era introduced in the software that controls the equipment. Data is analysed using the Universal Analysis 2000 software provided by TA Instruments Inc. The software calculates the values of enthalpy change and respective temperatures, heat capacity change and glass transition temperatures (all of this are collected in triplicate to decrease operator's error). An example of how the glass transition temperatures are collected, is shown in figure 16.

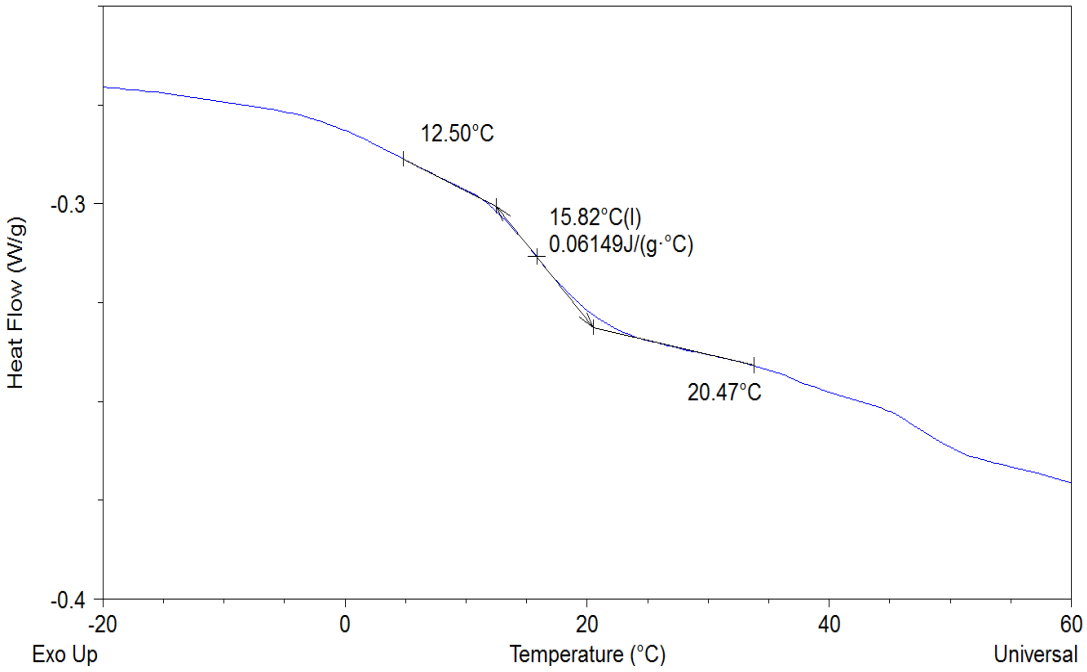

Figure 16. Illustration of how the temperatures are extracted at onset, midpoint and endset of glass transition.

Thermal treatments applied to the samples being studied are shown below:

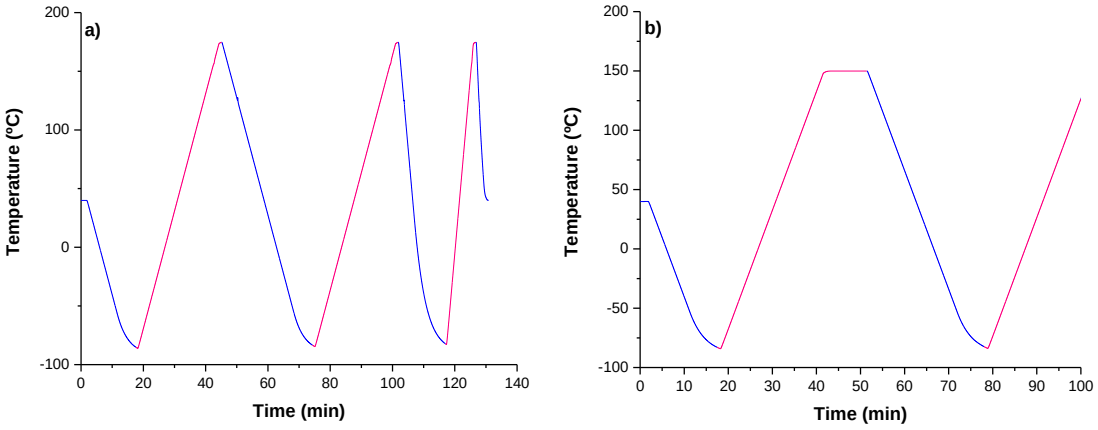

Figure 17. Thermal treatment applied to a) native naproxen and b) both silicas, in red heating cycles and in blue cooling cycles.

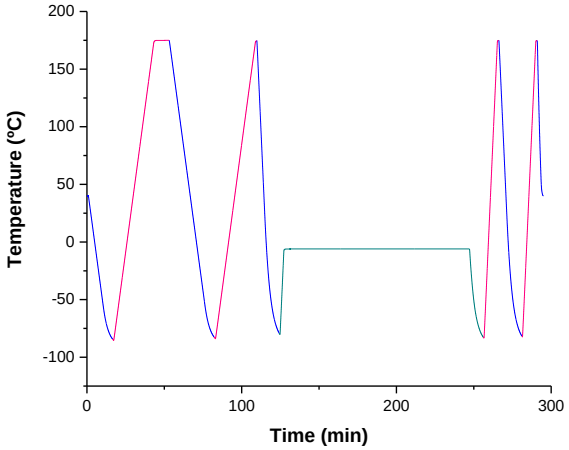

Figure 18. First Thermal treatment applied to both loaded composites in red heating cycles, in blue cooling cycles and in green annealing cycle.

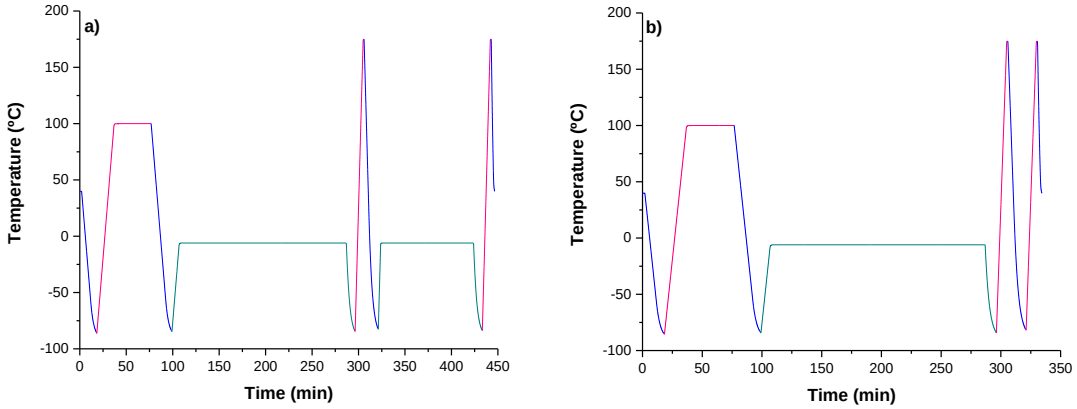

Figure 19. Thermal treatment applied to a) MCM-41 loaded with naproxen, b) MCM-41_Func loaded with naproxen, in red heating cycles, in blue cooling cycles and in green annealing cycles.

2.11 Dielectric Relaxation Spectroscopy (DRS)

A sample of both composites, MCM-41 and MCM-41_Functionalized, loaded with naproxen was placed between two gold-plated electrodes of parallel plate capacitors, BDS 1200 with two silica spacers (50 μm of thickness). The sample cell was placed on a cryostat, BDS 1100. The enclosed sample was submitted to a gas stream that came from the evaporation of liquid nitrogen, causing it to change temperature. Temperature control was ensured by Quarto Cryosystem and performed with 0.5 K. The software NovoControl Technologies GmbH supplied all the modules.

The measurements of dielectric relaxation were carried out using the Alpha-N independence analyzer from NovoControl technologies GmbH, covering a frequency range from 10^{-1} to 10^{6} Hz.

Both samples were submitted to a range of temperatures between -95 ºC to 170 ºC. To remove water/solvent evaporation from the sample, the last temperature for each first cycle was collected five times, ensuring that in the second heating the sample was completely dry.

Table 3. Temperature steps and range of dielectric measurements at which isothermal spectra were collected for both composites.

Sample	Temperature Range (ºC)	Temperature Steps (ºC)
MCM-41_naproxen	25 to -110	10
	-95 to 170	5
	-90 to 170	5
MCM-41_Func_naproxen	25 to -90	10
	-95 to 170	5

Data was analyzed and treated using WinFit and OriginPro Software using VFTH equation (see equation 7).

2.12 Control Release Experiments

Before all dissolution and control release trials were realized, a calibration curve is needed to quantify naproxen's concentration. Ten different naproxen's concentrations (0.1, 0.25, 0.5, 1, 2, 4, 5, 6, 8 and 10 mg L^{-1}) in buffer solution were prepared and measured over a wavelength range from 190 to 400 nm. Calibration curves were constructed by choosing 6 different wavelengths: 262, 272, 282, 330, 331 and 333 nm (see calibration curves in annex). The obtained linearity ($r^2 > 0.99$ for all the 6 chosen wavelengths) confirms the applicability of the Beer's law in the studied concentration range.

To simulate naproxen's dissolution rate, trials were realized by placing 1.0 mg of naproxen in 200 mL of phosphate buffer solution (concentration of 5 mg L^{-1}) at a pH= 6.8

(this is to simulate intestinal fluid, where naproxen is absorbed). The assays were performed in glass flasks in an Optic Ivymen System constant temperature incubator shaker (Comecta SA) regulated to 37 ºC (human body temperature) and 100 rpm.

In naproxen release experiments, calculi were done, to assure that the quantity of composite had the same amount of naproxen as the dissolution trials. Therefore, 1.0 mg of naproxen plus the mass of silica was placed in the phosphate buffer solution (200 ml). For every sample being analyzed (native naproxen, MCM-41_Naproxen and MCM-41_Func_Naproxen), the experiment was repeated three times, to decrease operators error.

An average of the concentration values obtained from the 6 calibration curves were used to estimate the concentration in the dissolution process.

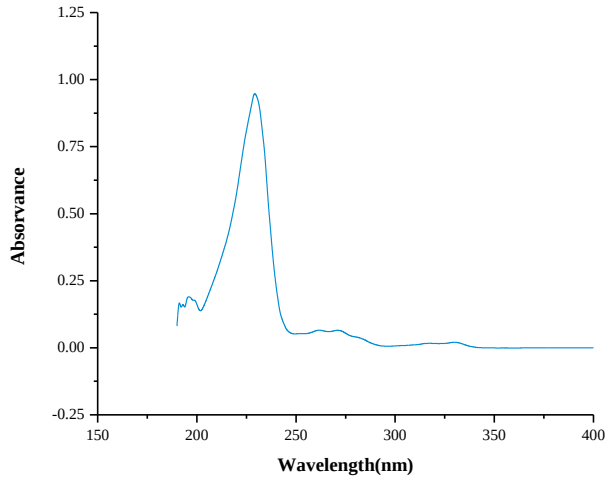

Figure 20. Naproxen UV-Vis spectrum

2.13 Ultraviolet-Visible Spectroscopy (UV-VIS Spectroscopy)

The sample absorptions were measured by UV-Vis at the wavelength range between 400 and 190 nm in quartz cells. The spectrometer was a Thermo Scientif Evolution.

3 Results and Discussion

3.1 Scanning Electron Microscopy (SEM)

From scanning electron microscopy, information about MCM-41, unloaded and loaded samples morphology was obtained.

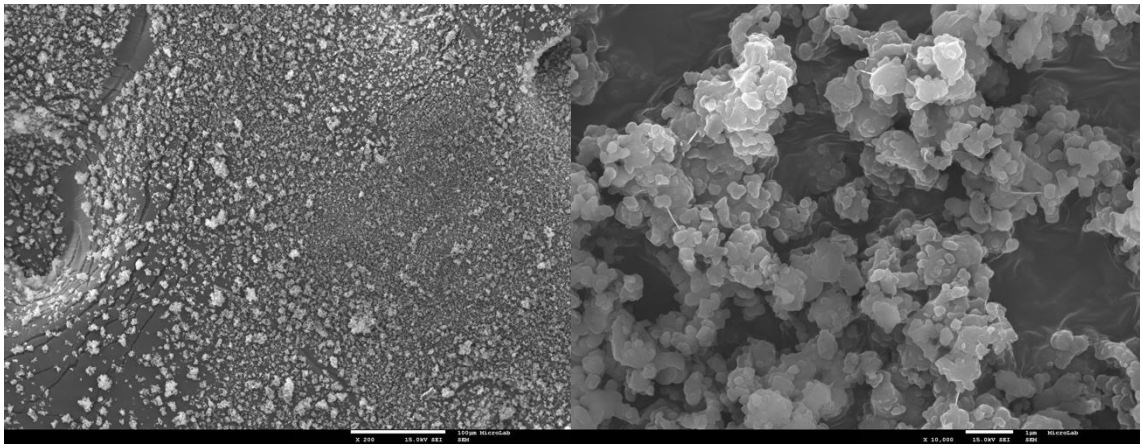

Figure 21. SEM Images of unloaded MCM-41. On the left, the image with an amplification of 200x and on right with 10.000x.

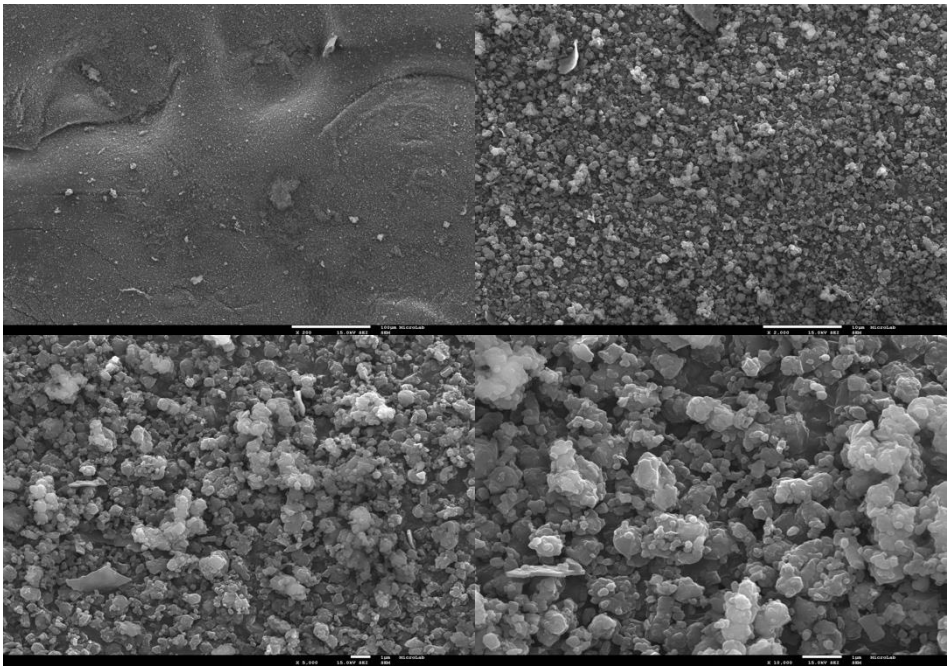

Figure 22. SEM images of loaded MCM-41. Top left 200x, top right 2.000x, bottom left 5.000x and bottom right 10.000x amplification.

As expected, the morphology of the MCM-41 silica is nearly spherical shaped, as is observed in the figures above (20 and 21). The aggregates formed from the silica particles are composed from regular particles and irregular ones.[22]

3.2 Transmission Electron Microscopy (TEM)

TEM images with textural characteristics of MCM-41 unloaded and loaded with naproxen are shown below:

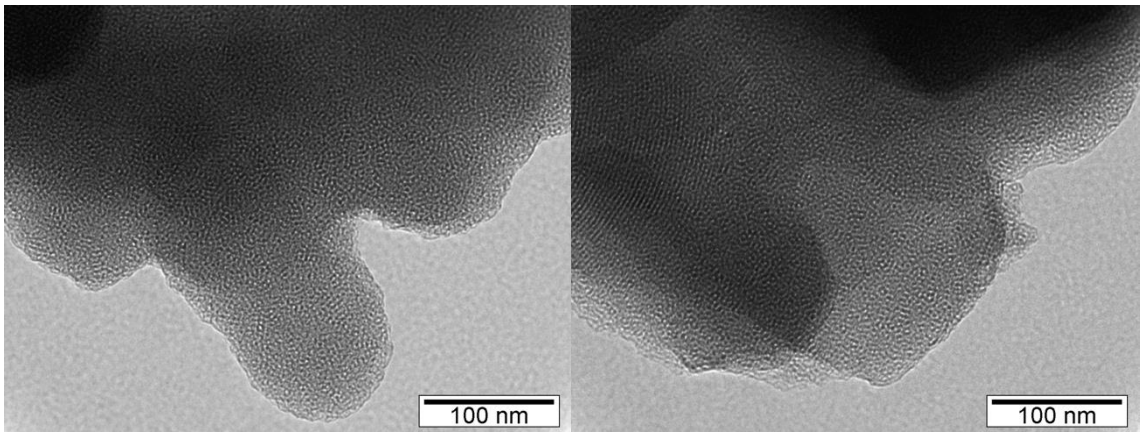

Figure 23. TEM micrographs of unloaded MCM-41.

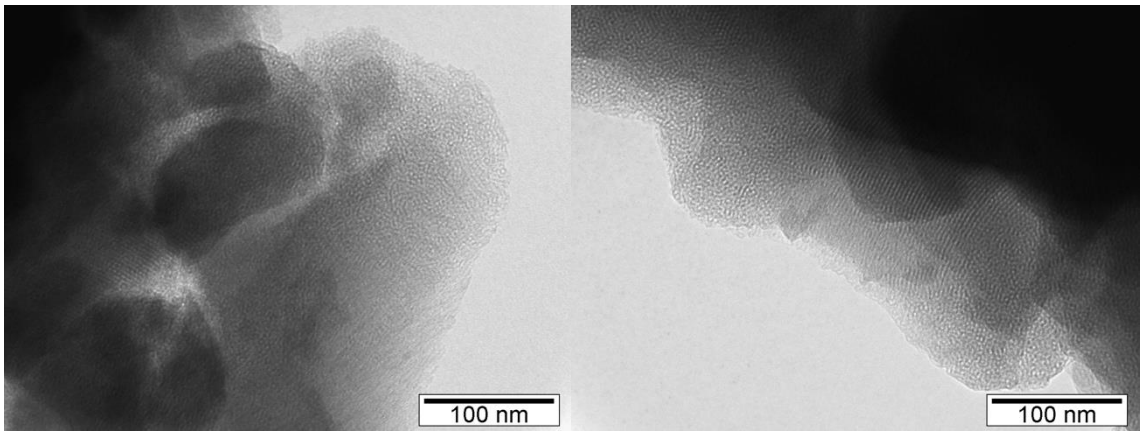

Figure 24.TEM micrographs of loaded MCM-41 with naproxen.

In the micrographs exposed above (figures 23 and 24), the order of mesoporous material is apparent. Also, it is perceptible the hexagonal shaped mesoporous with alternating channels and siliceous framework. [25]

3.3 Thermogravimetric Analysis (TGA)

TGA analysis for both matrixes, unloaded and loaded and for native naproxen is presented below figure 25.

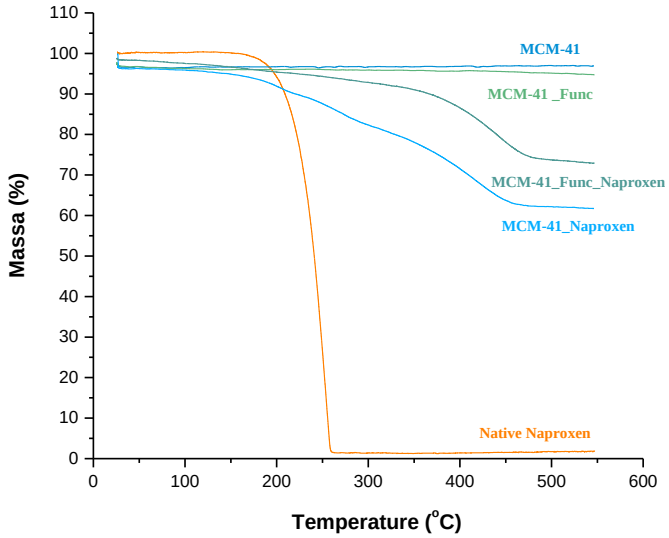

Figure 25. TGA plots for native naproxen (orange), both unloaded MCM-41(dark blue) and MCM-41_Func (light green) and the respective composites (light blue and dark green).

The unloaded matrixes MCM-41 and functionalized MCM-41 are thermally stable in the range of temperatures set in the apparatus; the small variances in both masses are due to water/solvent evaporation. In the modified silica, a small decomposition is observed ~350 ºC, due to the degradation of the organic functional groups.[46] The values for water content in both silica and respective composites, were obtained by subtracting the mass percentage at 150 ºC from the initial mass percentage.[46] For the organic functional groups in MCM-41_Func determination, the mass percentage loss was obtained in the range of 150 ºC and 550 ºC.[46] To calculate the loading percentages, equation 9 was used. These values are shown in table 4.

As the matrixes are stable in the programmed temperature, the only mass variation observed for the composite belongs to naproxen. Native naproxen is stable up to ~165 ºC (orange solid line 24), after starts do degrade in a single step, ending before ~275 ºC. From the thermogram of loaded matrices, naproxen becomes more thermal resistant when incorporated in the silica. The mass loss occurs in a multiple-step profile for the non-functionalized composite, not so evidently, the same is observed in the functionalized

one. The derivative plot shown in figure 25, demonstrates this multiple-step profile, giving evidence that the decomposition of naproxen is not linear.[4] This behaviour is attributed to bulk-like molecules (lower temperatures), and naproxen molecules which interact with pore walls (higher temperatures).[4]

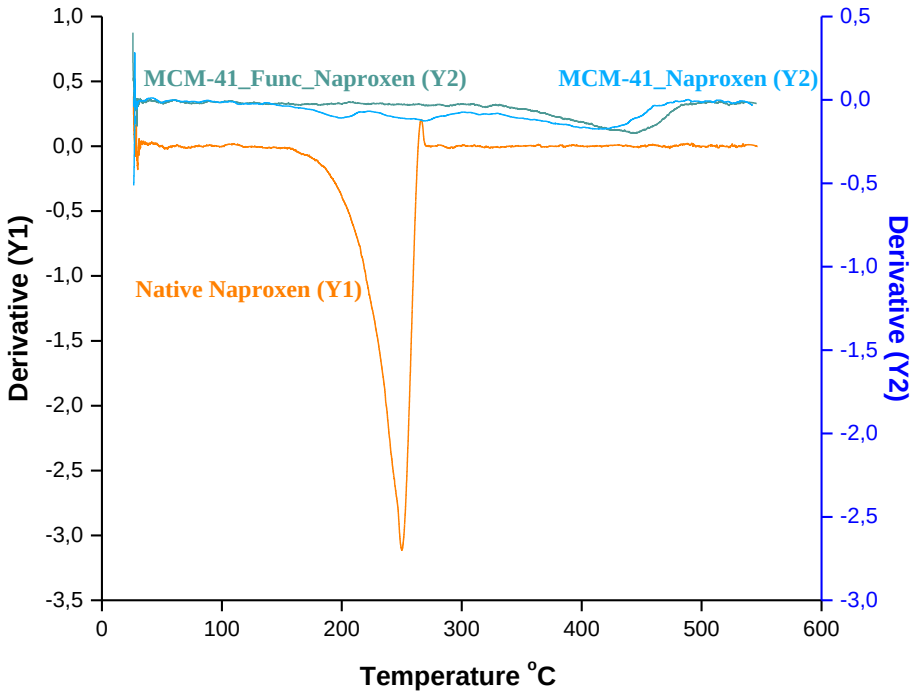

Figure 26. Derivative plot of native naproxen (orange), both loaded MCM-41 (bluw) and MCM-41_Func (green).

Using the equation 1 already mentioned before, the loading percentages of naproxen in the composite for MCM-41 and functionalized MCM-41, are 38.32 % and 27.09 % respectively. The percentage of naproxen in the silica for MCM-41 is 62.13 % and for functionalized MCM-41 is 37.16 %. The loadings for the MCM-41 are more compatible with the initial mass weight (80 %) used for loading, while the results for the functionalized MCM-41 are lower. This is probably due to a lower vacuum applied during the loading experiments for the latter.

Table 4. Water content, organic functional groups and loading percentages for both silica and composites.

	MCM-41	MCM-41_Func	MCM-41_Naproxen	MCM-41_Func_Naproxen
Water (% w/w)	0.51	1.71	5.12	2.14
Organic functional groups (% w/w)	-	1.26	-	1.26
Naproxen in the Composite (% w/w)	-	-	38.32	27.09
Naproxen in the composite (% v/v)	-	-	56.66	41.73
Naproxen in 100 g silica (% w/w)	-	-	62.13	37.16

3.4 Attenuated Total Reflectance Fourier Transform Infrared Spectroscopy (ATR-FTIR)

To analyze in more detail the functionalization on the MCM-41 matrix, cuts of ATR-FTIR spectra were done, so bands could be more easily identified. There are three ranges of wavelength where evidence of functionalization is supposed to be clearer: one between 4000-3500 cm^{-1} due to surface silanol types. The second from 3200-1200 cm^{-1} related to the presence of $-CH_3$ groups and the last being from 1400-400 cm^{-1} showing the different types of Si-O-Si and Si-OH vibrations.

Concerning the region between 4000 and 3500 cm^{-1}, the bands of interest are: i) the one located at 3742 cm^{-1} corresponding either to free isolated (Si-OH) or geminal silanol groups (HO-Si-OH)[36,47,48] and ii) at 3662 cm^{-1}, where the vicinal silanols (HO-Si-Si-OH) absorb[48], (see 27). The broader and relative weak band from 3925 to 3800 cm^{-1} is attributed to a combination of the stretching (υ) and torsional (τ) modes. In this close-up, the matrixes show no great differences.

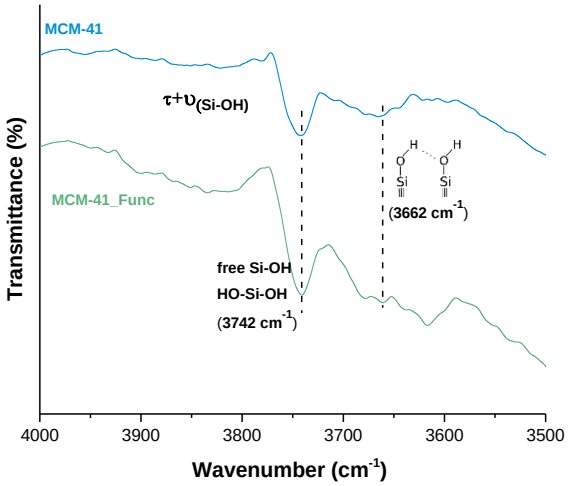

Figure 27. Region of the spectrum between 4000 and 3500 cm^{-1} for both matrixes, in blue the unmodified and in green the modified one. All the curves were vertically displaced for a better visualization. The dashed lines included to aid band visualization.

The next wavenumber window to be analyzed is in the range 3600 to 1200 cm^{-1}. Evidence of stretching vibrations of hydrogen bonded water molecules and Si-OH groups[47] in the range of 3600 to 3200 cm^{-1} are identified and it is a bit more pronounced in the functionalized silica; also for the later matrix, the peak at 1625 cm^{-1} due to water deformations is more intense.[47] These results agree with TGA water content that is higher for the functionalized silica (see Table 4). The bands at 2988 cm^{-1} and 2900 cm^{-1} results from asymmetric and symmetric stretching vibrations of C-H bonds, which are sharper in the MCM-41 C_{16} functionalized matrix; additionally, at 1399 cm^{-1} a weak band emerges due to Si-CH_3 bond vibrations.

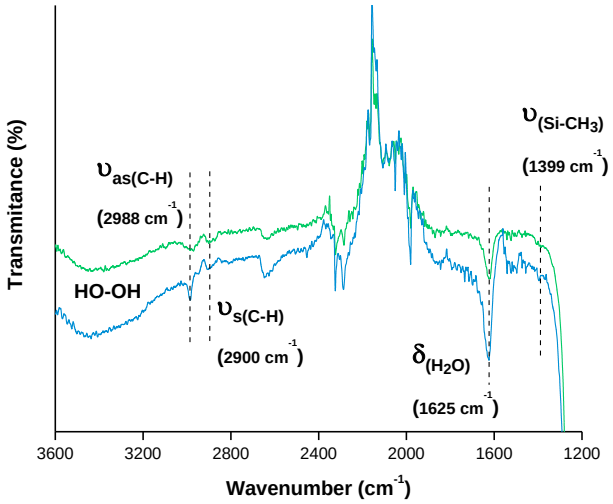

Figure 28. Region of the spectrum between 3600 and 1200 cm^{-1} for both silica, in blue the unmodified and in green the modified one. All the curves were vertically displaced for a better visualization. The dashed lines to aid band visualization.

The cut of the spectrum from 1400-400 cm^{-1}, several bands are identified due to Si-O-Si and O-Si-O, in general more intense in the functionalized matrix. From this, we can conclude that functionalization worked to some extent, as in all the zoomed areas of the spectrum, the Si-OH bands are always present in the MCM-41_Func, indicating that not all silanol groups in the surface were substituted by the functionalizing agent.[47]

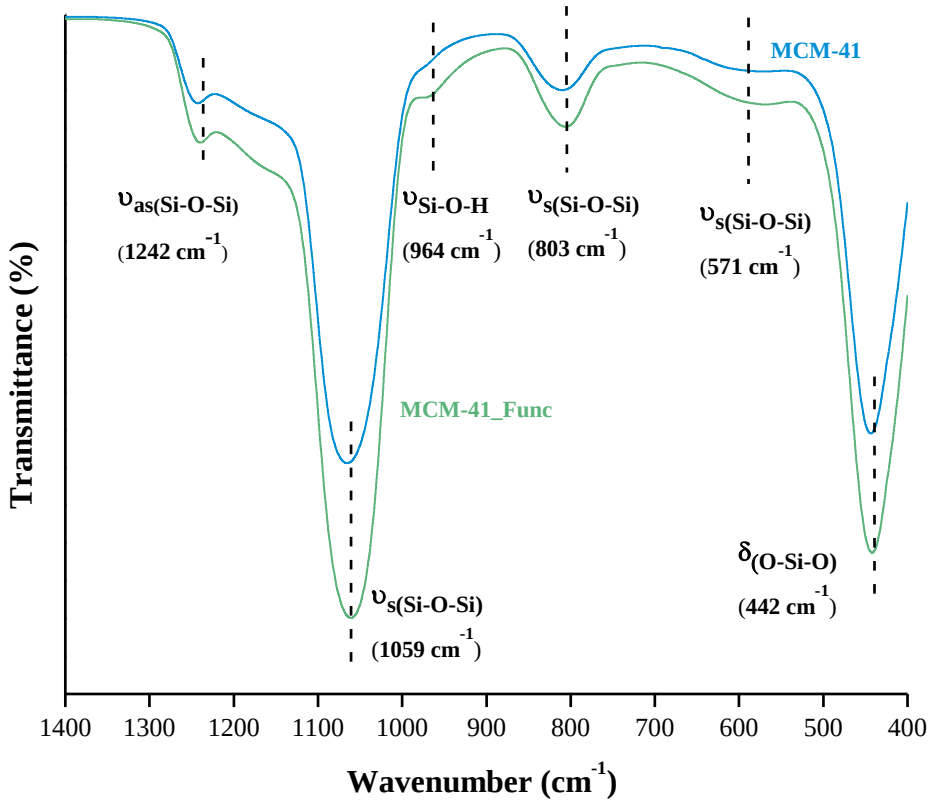

Figure 29. Region of the spectrum between 1400 and 400 cm^{-1} for the two matrixes, in green the unmodified and in blue the modified one. All the curves were vertically displaced for a better visualization. The dashed lines to aid band visualization.

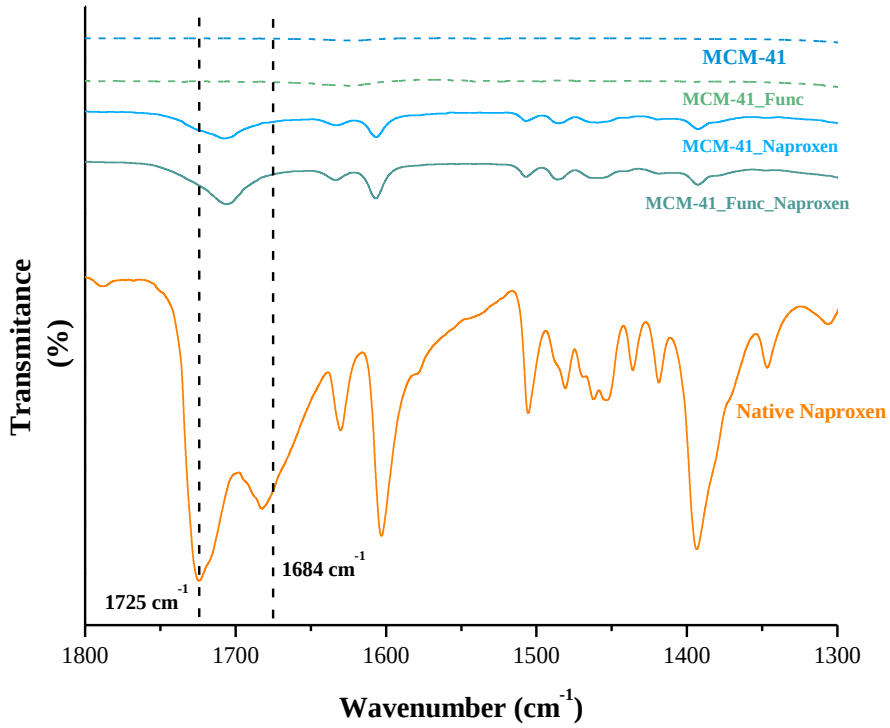

Figure 30. ATR-FTIR spectrum in the C-H, C=C and C=O regions for a comparison of native naproxen with the loaded and unloaded Matrixes of MCM-41 at room temperature. All the curves were displaced vertically for a better comprehension and visualization.

ATR-FTIR spectra were collected between the following frequency regions 1800 and 1300 cm^{-1}. The comparison between the unloaded matrixes, composites and native naproxen confirm successful loading. The loaded silica show response in the same areas as native naproxen. In the spectrum, there are two major regions that proof inclusion: the band near 1700 cm^{-1} due to C=O stretch and the band between 1300 and 1400 cm^{-1}, that is assigned to the coupling of aromatic rings, carbon-carbon stretching and C-H deformation modes in naproxen.[4] These absorption bands are not present in the unloaded silica.[23] When naproxen is in the crystalline state, the molecules interact with two adjacent molecules by hydrogen bonding and aromatic-aromatic interactions.[49,50] Hydrogen bonding interactions through the carboxylic groups occur due to the O-H or C=O bonds, leaving some free C=O groups because of their chain like structure.[51] So a significant region of the spectrum is the C=O stretching that is characterized by the bands at 1725 cm^{-1} representative of non-hydrogen-bonded C=O and 1684 cm^{-1} typical of the hydrogen-bonded C=O stretching.[51,52] In the spectrum of the composites, the band of free C=O of native naproxen is greatly suppressed and a broad band is registered at

1710-1705 cm^{-1}, this is caused by the hydrogen bonded C=O, that undergoes a shift to higher wave numbers as it is observed in quench cooled amorphous naproxen.[51] This can be taken as a first indication of amorphization, at least to some extent, because of the rearrangement from the chain like structure in crystal naproxen forming a dimer in the amorphous form.[51] The other appearing bands due to condensed polycyclic aromatic structure of naproxen in the range between 1600 cm^{-1} and 1440 cm^{-1} are less affected in the composites comparing to native naproxen, indicating that the arrangement of the aromatic parts do not undergo significant change and that it doesn't take part in the guest-host interaction, so it occurs via hydrogen bonds.[4] The spectra of the loaded matrix and unloaded matrix show a broad band at ~3400 cm^{-1}, which is due to physical absorption water.[23]

3.5 Nuclear Magnetic Resonance (NMR)

The solid-state NMR spectra probing Si chemical shift (^{29}Si -NMR) were deconvoluted in the individual Q^3 (isolated and vicinal silanol groups) and Q^4 (siloxanes) contributions (see figure 10). While in the untreated silica both Q^3 and Q^4 bands are present in the overall spectrum, in the treated silica only Q^4 was identified. The enhancement of siloxanes groups agrees with what was observed by ATR-FTIR (figure 29), being interpreted as a consequence of functionalization. See figure 31 and table 5.

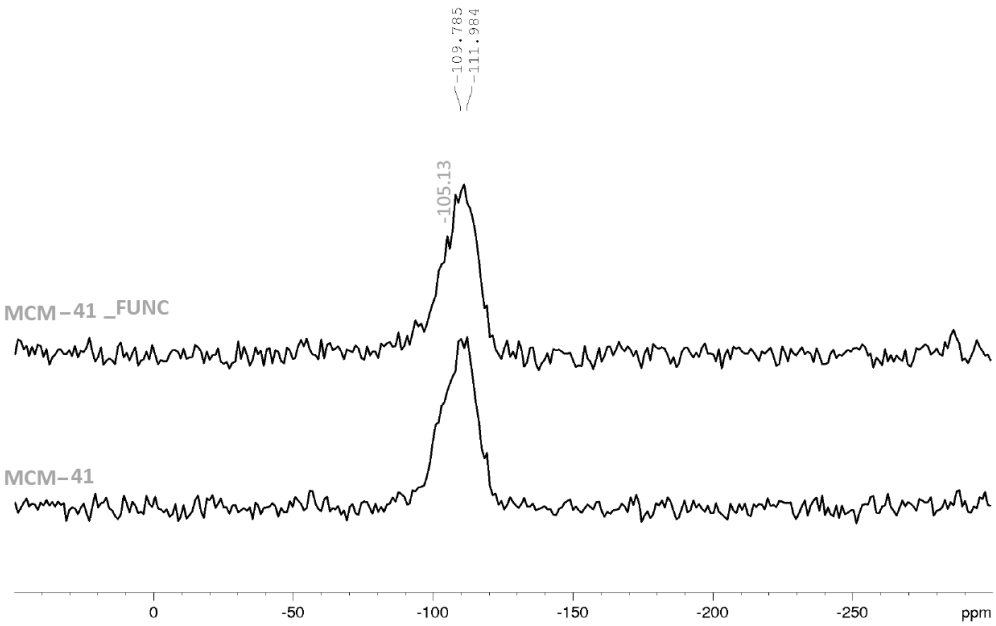

Figure 31. ^{29}Si MAS NMR spectra of the unloaded silica matrixes (see legend).

Table 5. Percentage and Chemical shifts of deconvoluted ^{29}Si MAS NMR spectra of MCM-41 and MCM-41_Func.[25]

	Q^2	Q^3	Q^4
MCM-41	-	-105 ppm 31 %	-111 ppm 69 %
MCM-41_Func	-	-	-111 ppm 100 %

To aid the confirmation of successful incorporation of methyl groups in silica surface, a ^{13}C NMR spectra is shown (figure 32).

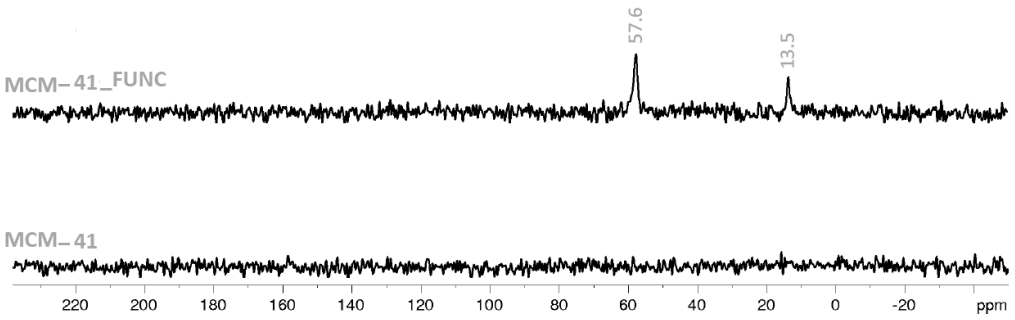

Figure 32. ^{13}C NMR spectra of MCM-41 and MCM-41_Func.

The emerging of the peak located near 57.6 ppm in the functionalized silica, absent in the unmodified one, evidences the presence of methoxy groups bonded to silicon (Si-O-CH_3)[25]. This can be taken as a sign of successful capping by methyl groups. However, the peak with the chemical shift at 13.5 ppm is identified as (Si-O-CH_2-CH_3)[25], due ethanol residues used to wash the functionalized silica.

3.6 Different Scanning Calorimetry (DSC)

The analysis by the DSC started with the study of the thermal behavior of the native naproxen. The thermogram below (figure 33) indicates two processes; in pink (1st heating) corresponds to melting, an endothermic event demonstrating an enthalpy variation of, ΔH_m= 130.86 J/g, the corresponding temperature is T_m= 156.73 ºC. These results agree with those reported in literature.[4] Upon cooling (in blue) crystallization is detected with a positive loop, the corresponding temperature being T_c= 127.24 ºC. Crystallization is an exothermic process, the variation in enthalpy is ΔH_c = -118 J/g. As the heat flow returns to base line before the equilibrium between the sample's temperature and the sensor's temperature is regenerated a hysteresis loop is formed.[4]

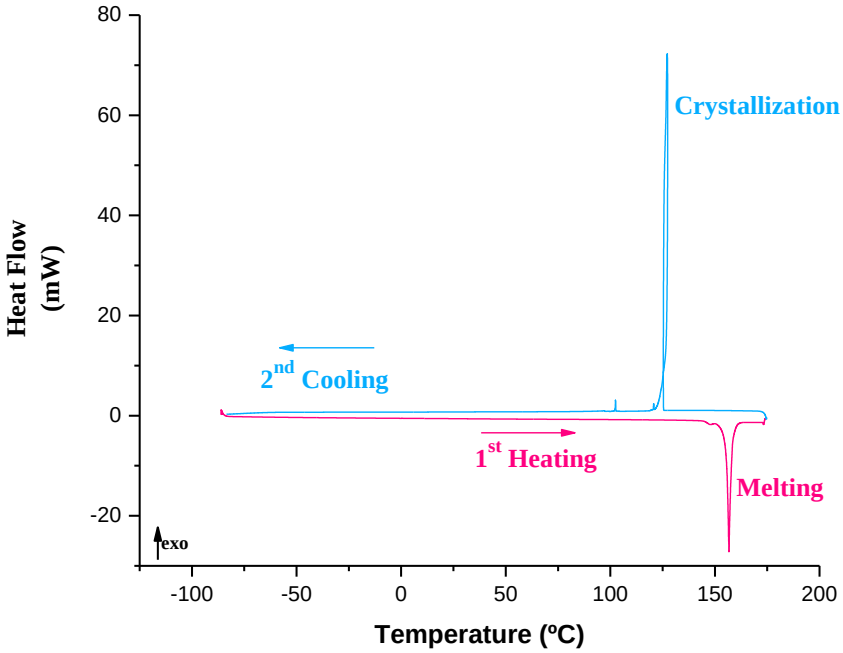

Figure 33. Thermogram of native naproxen, main cycles represented. In pink the first heating cycle followed by de second cooling cycle in blue.

Unloaded MCM-41 and MCM-41_Func were also calorimetrically characterized. In the first heating, an intense and broad endothermic peak centered at ~60/65 ºC due to water/solvent evaporation is registered, which is absent in the second heating (lighter pink) showing that all the water has evaporated, for both matrixes. Moreover, in the latter thermogram (figure 34) neither melting/crystallization or glass transition are detected, meaning the silica does not respond to any thermal treatment.

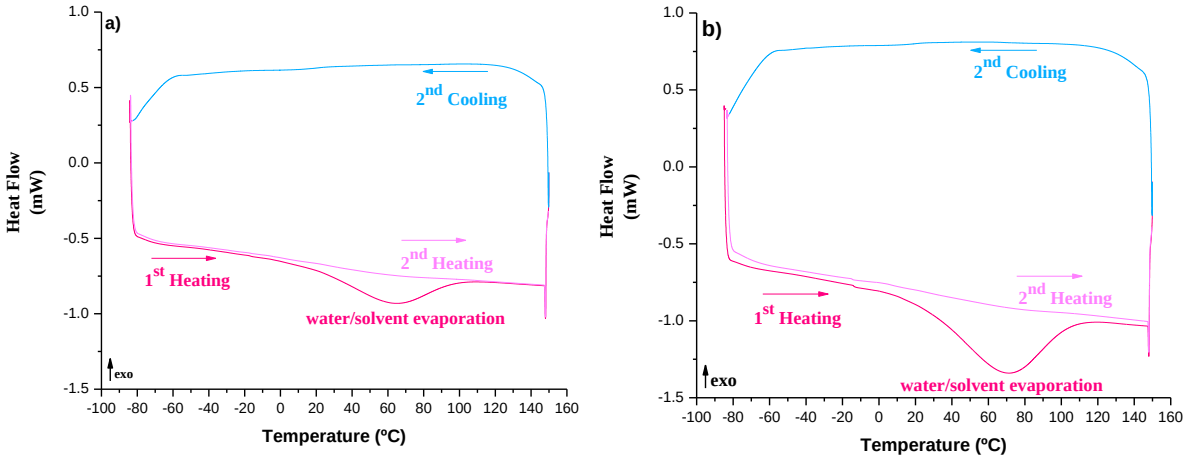

Figure 34. Thermogram of unloaded a) MCM-41 and b) MCM-41_Func, main cycles represented. In dark pink the first heating, second cooling cycle in blue followed by the second heating cycle in lighter pink.

The thermogram of MCM-41, loaded with naproxen is presented below. In the first heating cycle (dark pink) the characteristic behavior of naproxen is detected, a melting peak emerging at the same location of native naproxen T_m= 156 ºC, indicating there is a small fraction of the drug outside the silica's pores.[4] However, the melting peak is only present in the first heating cycle and the process of crystallization is never shown, demonstration that all naproxen stayed amorphous after the thermal treatment. To assure there is some drug inside the pores, an annealing treatment was carried out by keeping the sample for two hours at the temperature of -6 ºC (following the adopted procedure[4]). In the subsequent run (at a superior heating rate, 30 ºC/min), a step emerges in the heat-flux signal ~0 ºC, which is the signature of the glass transition (light pink, after annealing), demonstrating amorphous naproxen.

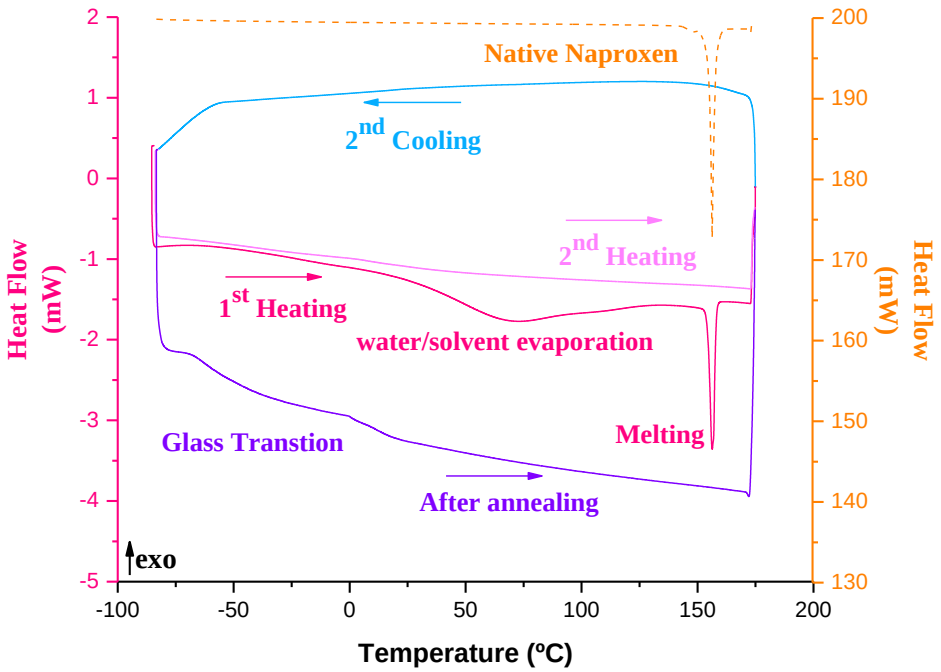

Figure 35. Thermogram of loaded MCM-41, main cycles represented. In dark pink the first heating cycle and native naproxen heating cycle, the second cooling cycle in blue, second heating cycle in lighter pink followed by the cycle after annealing in purple. Native naproxen curve in orange was displaced vertically for a better comprehension and visualization.

Table 6. Table showing values of enthalpy variation and melting temperature for MCM-41 incorporated with naproxen with no framework, the following values are an average from three collections.

Melting Temperature (ºC)	$\Delta H_{melting}$ (J/g)
156.27	8.866

This same sample was analyzed two months later, demonstrating all the naproxen was stabilized in the amorphous form.

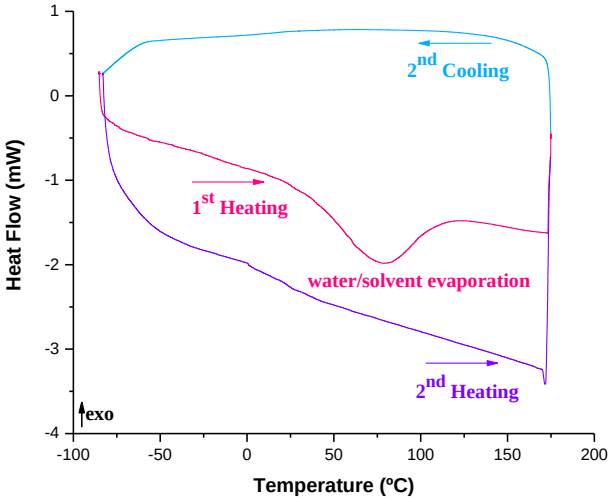

Figure 36. Thermogram of loaded MCM-41_Naproxen two months after the first reading, main cycles represented. In dark pink the first heating cycle, the second cooling cycle in blue, second heating cycle in purple.

Since the glass transition was only characterized after melting of the outsider crystalline fraction, it is influenced by the amorphization of bulk-like naproxen. To have a better insight of amorphous portion inside the pores, that resulted directly from incorporation, a new sample was analyzed, using a different procedure: 1) water removal at a temperature (100 ˚C) so there was no interference with any process of naproxen (T_m = 156 ºC); 2) annealing at -6 ºC prior to melting; 3) annealing at -6 ºC after melting. (see scheme 19a) in experimental section).

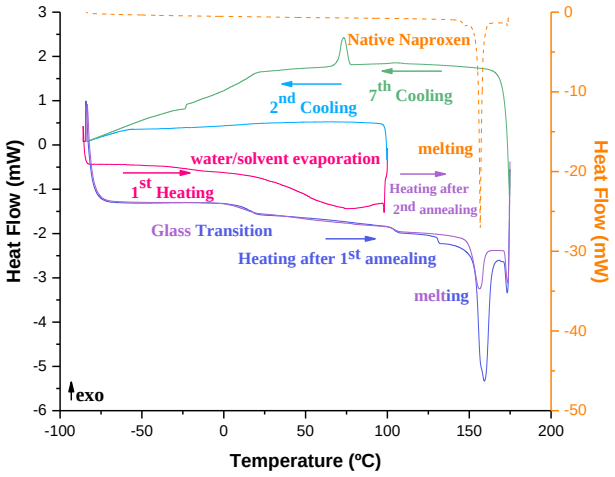

Figure 37. Thermogram of loaded MCM-41, main cycles represented. In dark pink the first heating cycle, in orange native naproxen heating cycle, the second cooling cycle in blue, heating cycle after annealing in dark blue, heating cycle after second annealing in purple, seventh cooling cycle in green. Native naproxen curve was displaced vertically for a better comprehension and visualization.

After water removal and annealing cycle, the glass transition becomes more evident (Figure 37); the onset, midpoint and endset values are presented in **table 7.** The latter are higher, by comparison with T_g values for incorporated naproxen in similar silica hosts[4], indication a strong constraining inside pores. Additionally, melting occurs at the same temperature as the native, which is evidence of naproxen outside the pores meaning not all naproxen was amorphous after the incorporation. Also, a fraction of naproxen recrystallizes as there is a crystallization peak in the cooling ramp after (7^{th} cooling cycle). After the second annealing (violet cycle), the glass transition shows a slight shift to lower temperatures (better seen in the derivative plot figure 38), probably resulting from a superposition of already incorporated naproxen and a new amorphous bulk-like fraction.

Table 7. Values of thermal transitions collected from DSC for unmodified loaded composite, MCM-41_Naproxen. The data result from an average of three collections.

	MCM-41_Naproxen
T_g (onset) ºC	9.33
T_g (midpoint) ºC	17.49
T_g (endset) ºC	20.24
ΔCp (after first annealing cycle) (J/g ºC)	0.12
$\Delta H_{melting}$ (after first annealing cycle) J/g	8.63
$T_{melting}$ (after first annealing cycle) (ºC)	159.18
$\Delta H_{melting}$ (after second annealing cycle) J/g	2.40
$T_{melting}$ (after second annealing cycle) (ºC)	155. 94

T_g is shown in figure 38, the derivative was also plotted, demonstrating the shift from between populations.

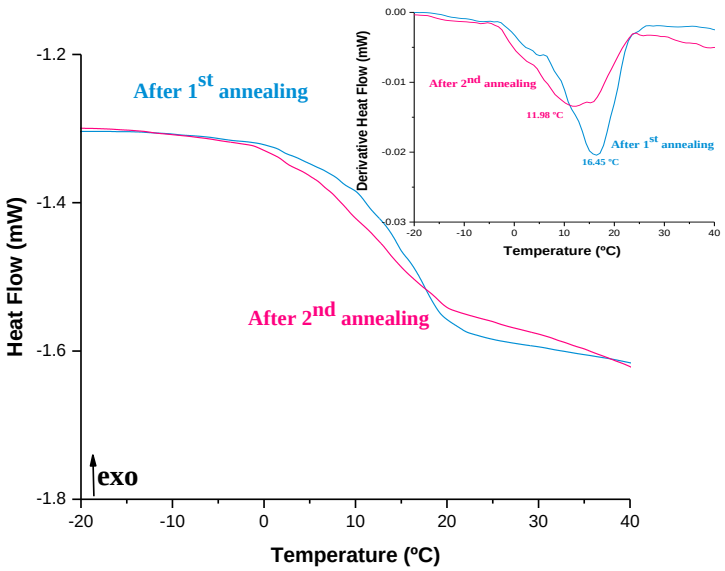

Figure 38. Thermogram of loaded MCM-41, derivative plot evidencing one populations, smoothing was applied (x15).

The results obtained from the first reading of functionalized MCM-41 incorporated are represented in the thermogram below. Once more in the first heating cycle (dark pink) the distinctive behavior of naproxen is shown with the melting peak at the temperature T_m= 156 ºC, indicating that naproxen was not completely amorphous by incorporation, only after thermal treatment.[4]

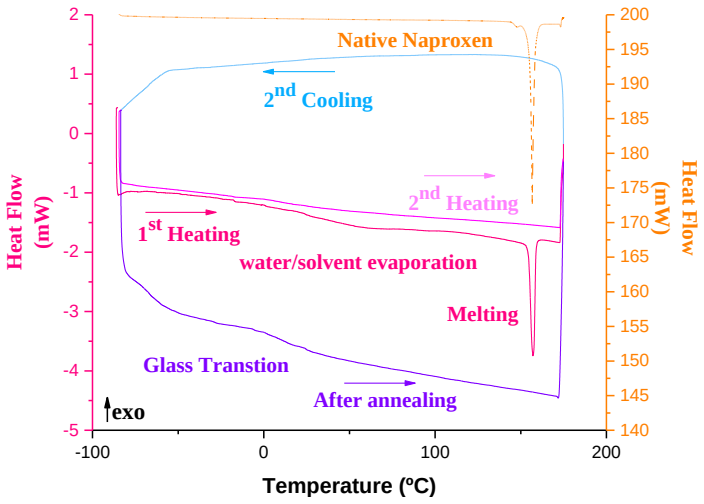

Figure 39. Thermogram of loaded functionalized MCM-4, main cycles represented. In dark pink the first heating cycle and native naproxen heating cycle, the second cooling cycle in blue, second heating cycle in lighter pink followed by the cycle after annealing in purple. Native naproxen curve in orange was displaced vertically for a better comprehension and visualization.

Table 8. Table showing values of enthalpy variation and melting temperature for functionalized MCM-41 incorporated with naproxen. The values result from an average of three collections.

Melting Temperature (ºC)	Enthalpy Variation (J/g)
157.09	**11.04**

As for the unmodified silica loaded with naproxen, the functionalized one was submitted to the same water removing treatment, but only one a three-hour annealing. The following thermogram figure 40 was obtained.

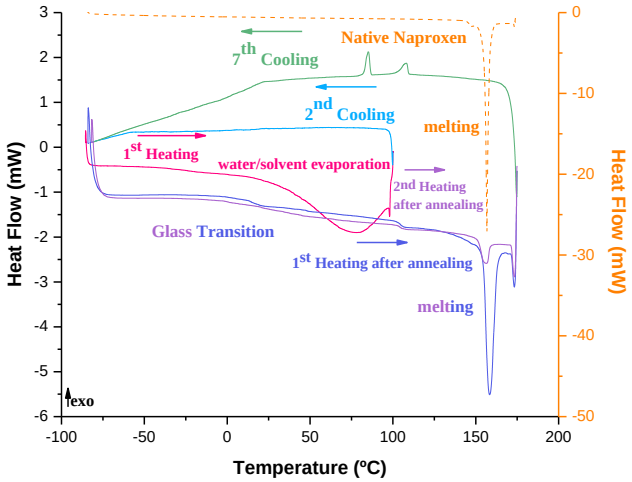

Figure 40. Thermogram of loaded functionalized MCM-41, main cycles represented. In dark pink the first heating cycle, in orange native naproxen heating cycle, the second cooling cycle in blue, heating cycle after annealing in dark blue, second heating cycle after annealing in purple, seventh cooling cycle in green. Native naproxen curve was displaced vertically for a better comprehension and visualization.

The three-hour annealing cycle, eased the gathering of the glass transition data. The thermogram shows melting once more, due to excess naproxen. Naproxen was not completely amorphous after incorporation after inclusion procedure, and after annealing cycles some recrystallizes as a crystallization peak is present in the cooling cycle after. The data obtained from the thermogram (figure 40) is shown in the table 9 below.

Table 9. Values of thermal transitions collected from DSC for modified loaded composite, MCM-41_Naproxen. The data resulted from an average of three collections.

	MCM-41 C_{16}_Naproxen
T_g (onset) ºC	8.79
T_g (midpoint) ºC	11.04
ΔCp (J/g ºC)	0.10
$\Delta H_{melting}$ (1^{st} heating after annealing cycle) (J/g)	9.139
$T_{melting}$ (after first annealing cycle) (ºC)	158.02
$\Delta H_{melting}$ (2^{nd} heating after annealing) (J/g)	1.27
$T_{melting}$ (2^{nd} heating after annealing) (ºC)	155.97

T_g and derivative plot for the MCM-41_Func_Nap is shown below.

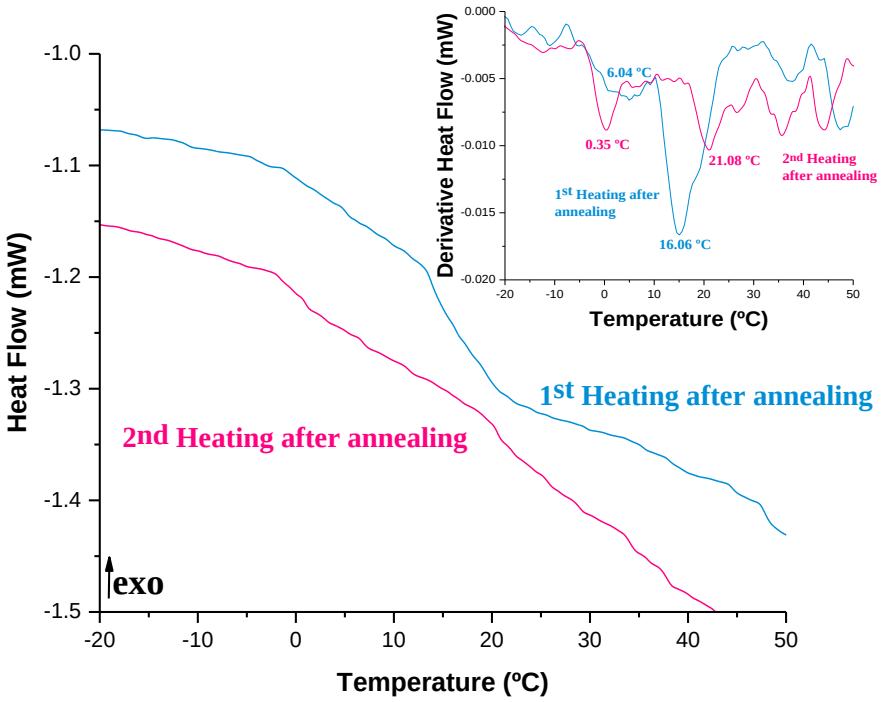

Figure 41. Thermogram of loaded MCM-41_Func_Nap, derivative plot evidencing one populations, smoothing was applied (x15).

The crystalline percentage was calculated for both composites. Using enthalpy values from DSC, corrections were made taking in account the water content and loading (obtained by TGA) to obtain crystalline percentage.

Table 10. Crystalline Percentage calculi for both loaded matrixes.

	MCM-41_Naproxen	MCM-41_FUNC_Naproxen
DSC sample weigh (mg)	4.30	3.95
$\Delta H_{melting}$ (1st heating after annealing cycle) (J/g)	25.08	35.51
% Crystallinity (1st heating after annealing cycle)	6.59	6.98
$\Delta H_{melting}$ (2nd heating after annealing) (J/g)	-	5.073
$\Delta H_{melting}$ (after 2nd annealing) (J/g)	6.98	-
% Crystallinity (2nd heating after annealing)	1.83	0.97

A comparison between the two dehydrated composites was realized, after the annealing before melting, to evaluate if the behavior differed. Figure 42 compares the glass transition region; a) conventional heat-flux plot and b) derivative plot. While in a) no major differences are noted, their distinction becomes clear in the derivative representation b). Two populations are distinguished for the modified silica, one more mobile at lower temperatures and a more hindered one at higher temperatures, whereas a broader and less resolved is found for the unmodified one. These results are backed-up while analyzing dielectric relaxation data.

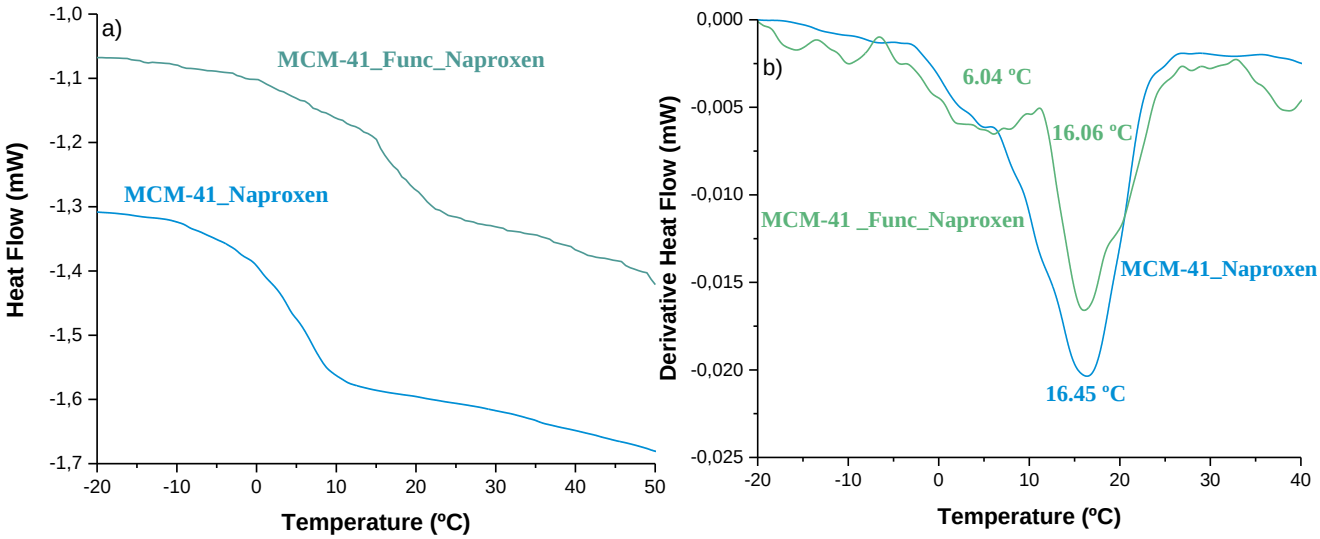

Figure 42. Comparison of both composites, after annealing (dried); a) T_g plot and b) derivative plot of T_g. In blue unmodified composite and in green functionalized composite.

3.7 Dielectric Relaxation Spectroscopy (DRS)

To evaluate the molecular mobility of incorporated naproxen, dielectric studies were carried, probing reorientation motions through the response of dipolar units (mainly the carboxylic moieties) to an oscillating external electric field.

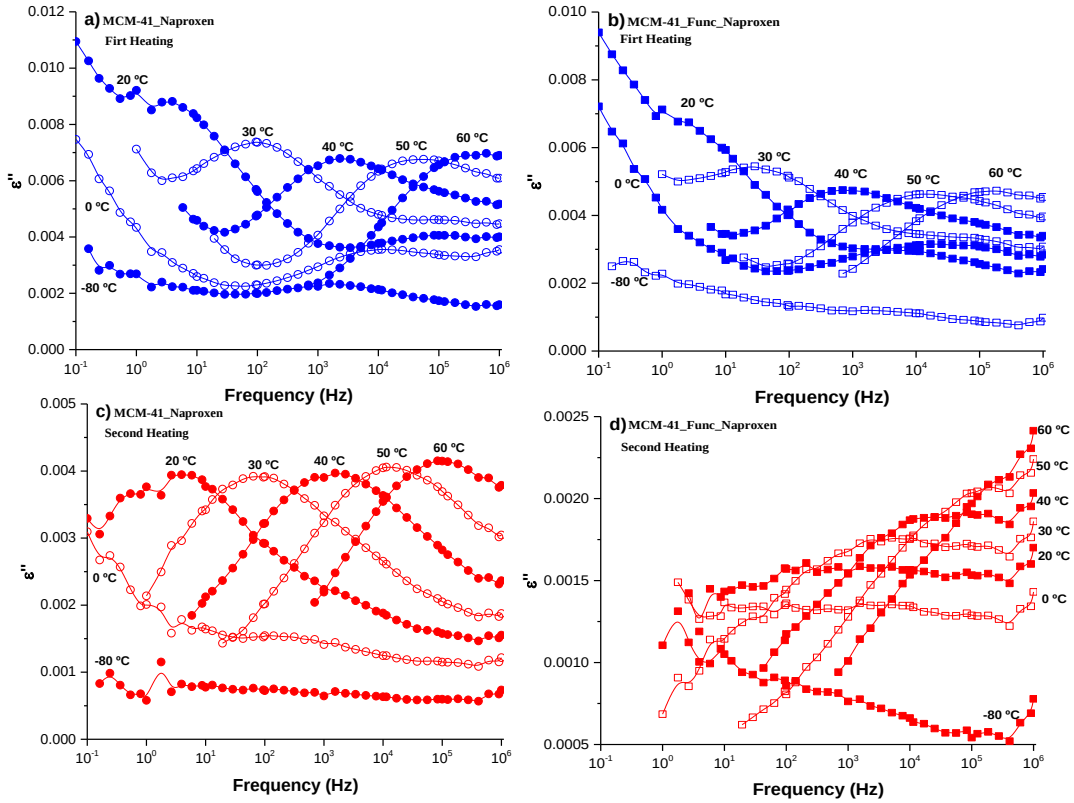

Figure 43. Dielectric loss spectra taken isothermally at the temperatures indicated for a) and b) hydrated (1st heating) and c) and d) dried (2nd heating) composites; see legend inside figure.

In figure 43, the composites dielectric response is expressed in terms of the imaginary component (dielectric loss) of the complex dielectric permittivity (see introduction). The dielectric loss spectra were taken isothermally, for the as prepared composites (hydrated-blue curves) and after water removal (dried-red). In general, with the temperature increase, the maximum of the ε´´-peaks show a shift towards higher frequencies. This is an expected effect, since rising the temperature enables molecular mobility. This is due to the inverse relationship between time and frequency: higher frequency means a lower relaxation time, i.e., faster relaxation rate. Moreover, for the hydrated composites (figure 43 a) and b)) the maximum intensity of the peaks, shows a

decrease with increasing temperature due to continuous water depletion. This occurs in such a way, that the response for the dried composites comes out highly suppressed. The remaining dielectric loss which is owing to incorporated naproxen under dry conditions is even weaker in the functionalized MCM-41 due lower filling degree, as given in table 4.

An alternative representation to ease the dielectric analysis is to plot data in function of temperature at a fixed frequency, this is fixed time (isochronous), being called isochronal plot. This is shown in figure 44 for both composites, a) unmodified and b) modified, for the frequency of $1x10^4$ Hz.

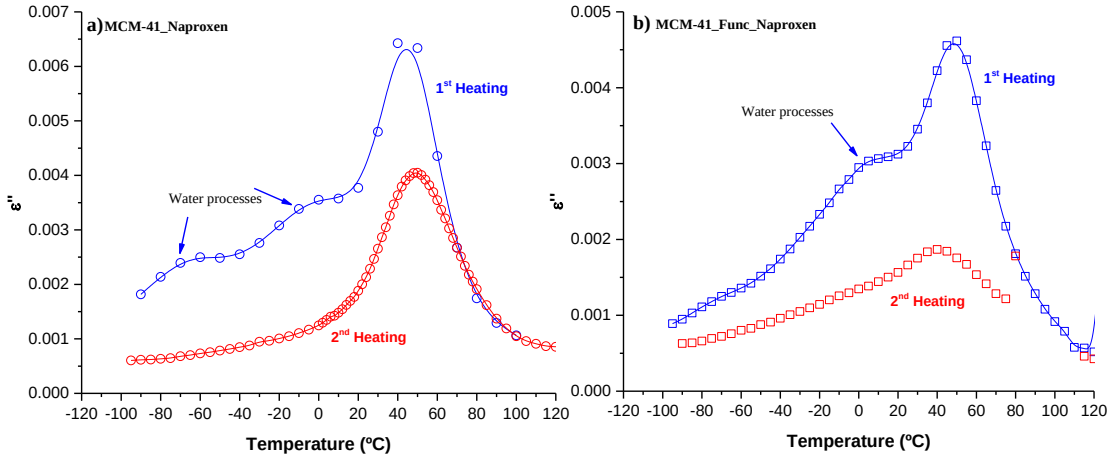

Figure 44. Isochronal plots at the frequency 1x104 Hz for composites, a) unmodified matrix and b) modified matrix. In blue hydrated cycle (1st heating) and in red, dried cycle (2nd heating).

As mentioned before, the decrease in magnitude of the dielectric response is clearly shown in both composites for the first heating comparing to the second one. This is due to the high dipolar moment of the water molecule as the thermal treatment removes water during the first heating. Furthermore, in the unmodified matrix, two relaxation processes are shown in blue (first heating cycle) at low temperatures that disappear in the second run (red) and therefore these are attributed to the relaxation of water molecules. This is not so evident in the functionalized MCM-41, most probably because, as discussed in the results of NMR and ATR-FTIR, the reduction of surface OH groups decreases the number of adsorption sites for water molecules.

To facilitate a comparative discussion between both composites in the two conditions, hydrated and dry, the following isochronal and isothermal plots will be analyzed.

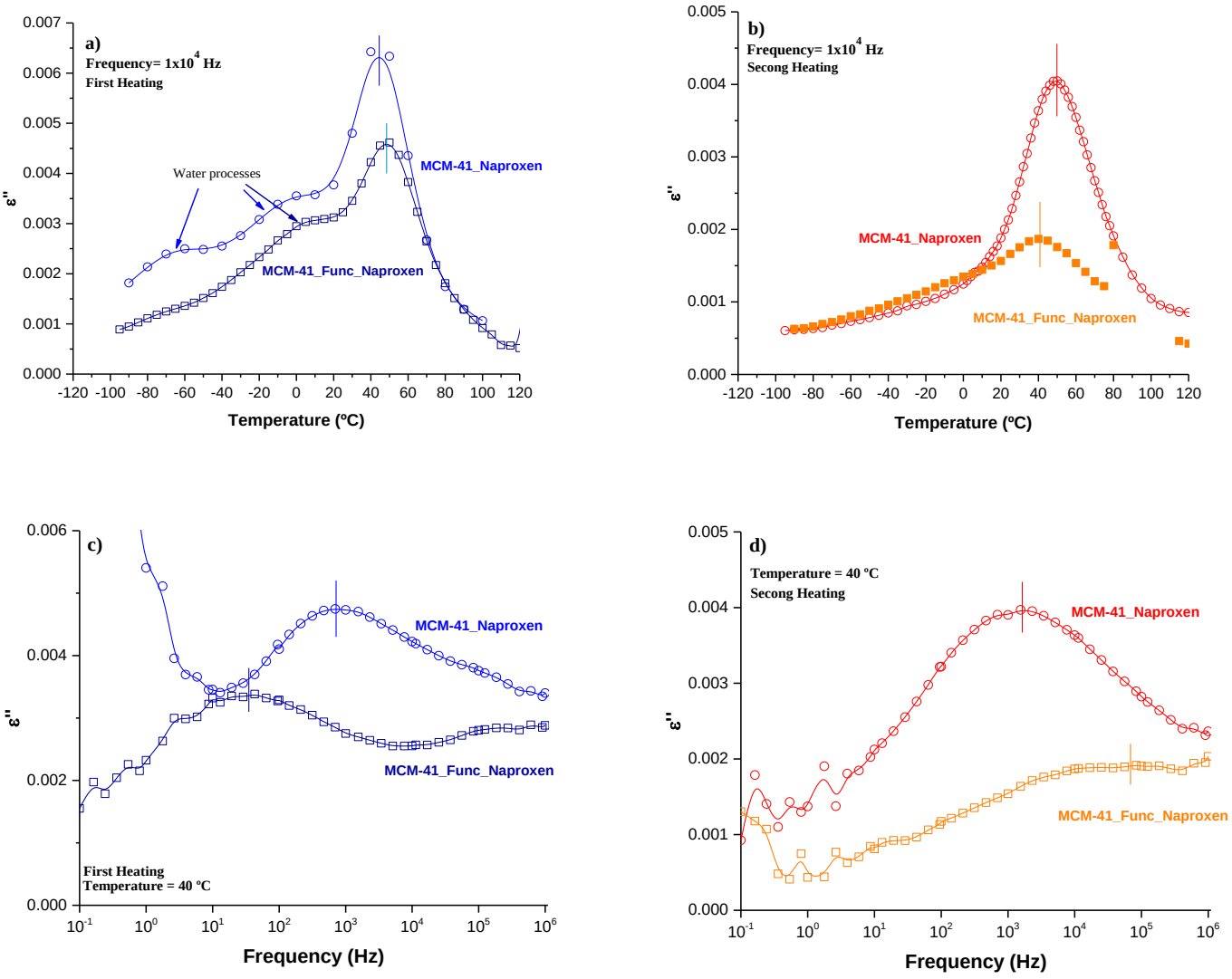

Figure 45. Comparative analyses between both composites for first and second heating cycles, through isochronal a), b) and isothermal c), d) representations.

In isochronal curve a), even if small, there is a shift to lower temperatures of the maximum peak of the unmodified composite to the maximum peak of the modified composite (small vertical bars aid visualization). This means naproxen's molecules have higher mobility in the MCM-41 than in the functionalized MCM-4. Also, the two water processes are more obvious, so probably the water molecules exert a plasticizing effect over naproxen enhancing its mobility. On the other hand, in the second heating (isochronal plot b) the two maximum peaks invert their position. Having the naproxen's molecules a higher mobility in the functionalized MCM-41, as at a frequency of $1x10^4$ Hz the maximum peak is located at lower temperatures. One of the hypotheses is, as the functionalized silica has $-CH_3$ instead of -OH groups at the pore walls, a decrease in the

guest-host interaction occurs, rendering the molecules more mobile. These outcomes are even more explicit while comparing the isothermal spectra.

A more detailed analysis was carried out with the loaded MCM-41 in the dried state (second heating). Since multiple relaxation processes are felt by the multimodal isothermal profile of the dielectric loss spectra, it was deconvoluted by using software Winfit from NovoControl. An example is shown in the figure 46 for the spectrum collected at 8 ºC.

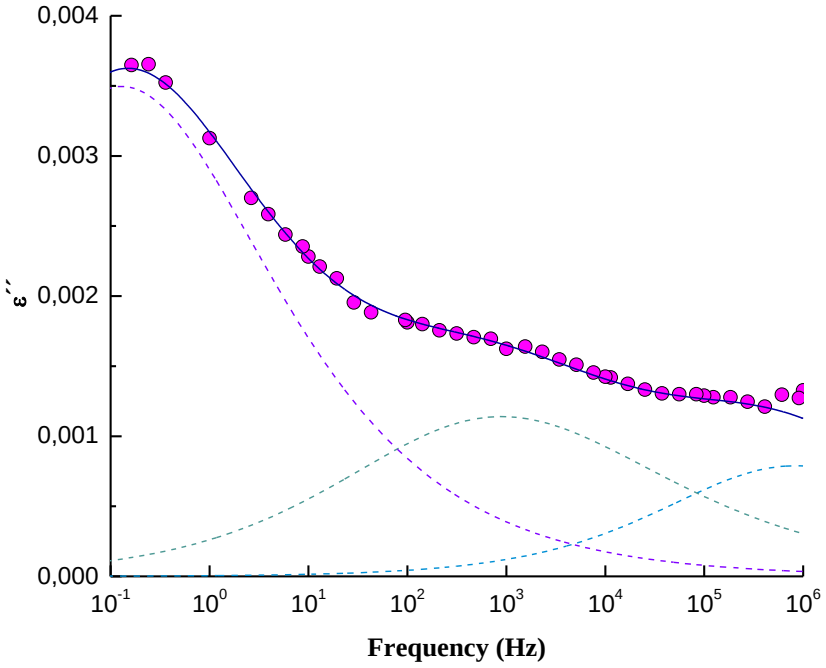

Figure 46. Representation of a fitting process.

The deconvolution illustrated in figure 46, shows that to obtain a proper simulation of the ε'' data, three HN-functions (equation 6) were used. The most relevant parameter that allows extracting dynamical information is the frequency of the maximum of each peak, from which the relaxation time is derived. Although three individual relaxation processes are felt, from now on, the analysis will only proceed with the process located at the lowest frequencies, the one to be believed associated with the glass transition, therefore designated alpha process, as mentioned in literature. The additional processes located at higher frequencies are related to more local mobility out of the scope of this project.

A plot of the relaxation times obtained for the alpha process for the loaded MCM-41 in function of the temperature reciprocal (open-pink circles) is shown in figure 47. This type of representation is known as relaxation map, which provides the dynamical fingerprint

of the system.[39] The plot also includes the data estimated from the isochronal representation (open-blue circles) from which the temperature of ε'' maximum at a fixed frequency is extracted. The relaxation time for each temperature is calculated from the frequency through the relationship $\tau=2\pi f$.

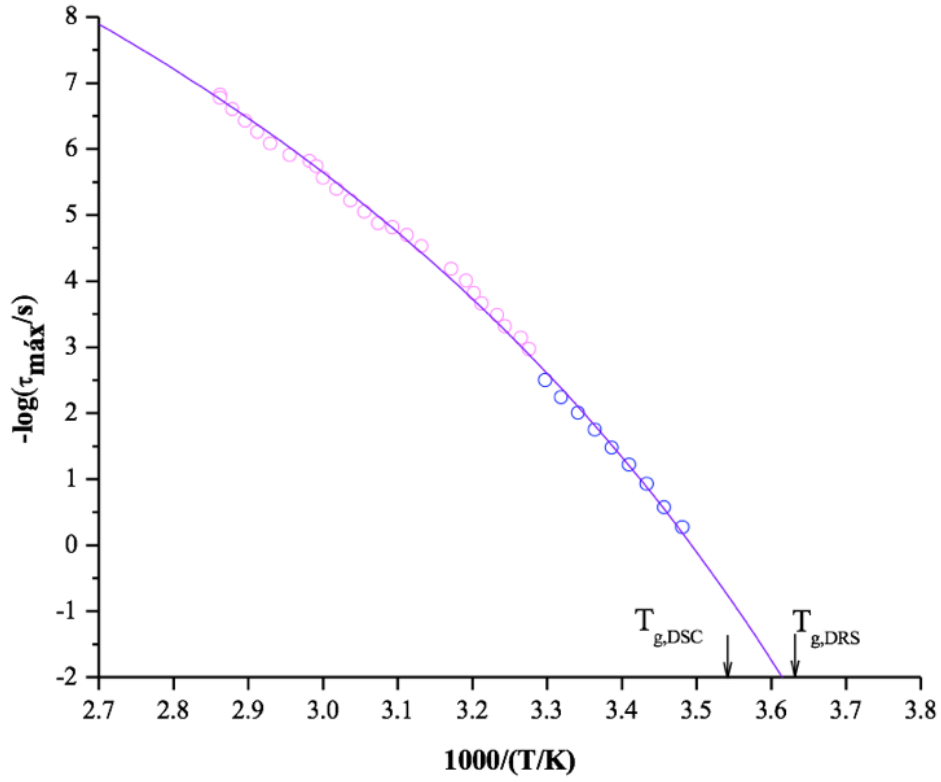

Figure 47. Relaxation time, τ, versus 1/T for the alpha process of the composite MCM-41, pink circles, isothermal loss data, blue circles, τ obtained from isochronal plots for some frequencies ($\tau=1/(2\pi f)$, $1/T_{max}$). The solid line is the VFTH fit to the data (see equation 7, and parameters in table 11). Arrows indicating dielectric $T_{g,DRS}$ (τ=100 s) and calorimetric $T_{g,DSC(onset)}$ glass transition temperatures.

In figure 47 it is obvious how the two sets of data follow the same tendency. Furthermore, the temperature dependence exhibits curvature, which is taken as an indication of cooperativity. Indeed, for localized process with short length scale an Arrhenius dependence is found due to a single activation energy. On the other hand, in cooperative processes the activation energy, Ea, is temperature dependent, increasing with temperature decrease, becoming more accentuated while approaching the glass transition temperature. The variation of Ea is interpreted as a consequence of increasing length scale of the molecular regions that rearranges in a cooperative manner with the temperature decrease.[39]

Table 11. Estimated parameters of the VFTH Fit to the relaxation times of the α-process for MCM-41 loaded with naproxen.

Parameters	α-relaxation
T_g(DSC) / ºC	9.33
τ_0 / s	7.76×10^{-16}
B / K	2765.9
T_0 / K	206.8
$T_{g,\ DRS\ (\tau=100\ s)}$ / K	277
$T_{g,\ DRS\ (\tau=100\ s)}$ / ºC	3.8
Ea (T_g) / kJ mol^{-1}	358

To take in account the curvature of the temperature dependence, a VFTH law was used (See equation 7) to obtain the respective parameters, which are provided in table 11.

According to the Maxwell relation, that correlates viscosity and the shear modulus G, though $\eta=G\tau$, a relaxation time of 100 s is obtained by assuming, for a solid material, a viscosity of ~10^{12} Pa s and G ~10^{10} Pa.[39] This gives an estimate of the glass transition temperature. The thus estimated Tg is 3.8 ºC is in reasonable accordance to the value estimated by calorimetry from the onset of the transition (9.33 ºC) corroborating the assignment of this process to the one driving the naproxen glass transition inside pores.

3.8 Control Release Experiments

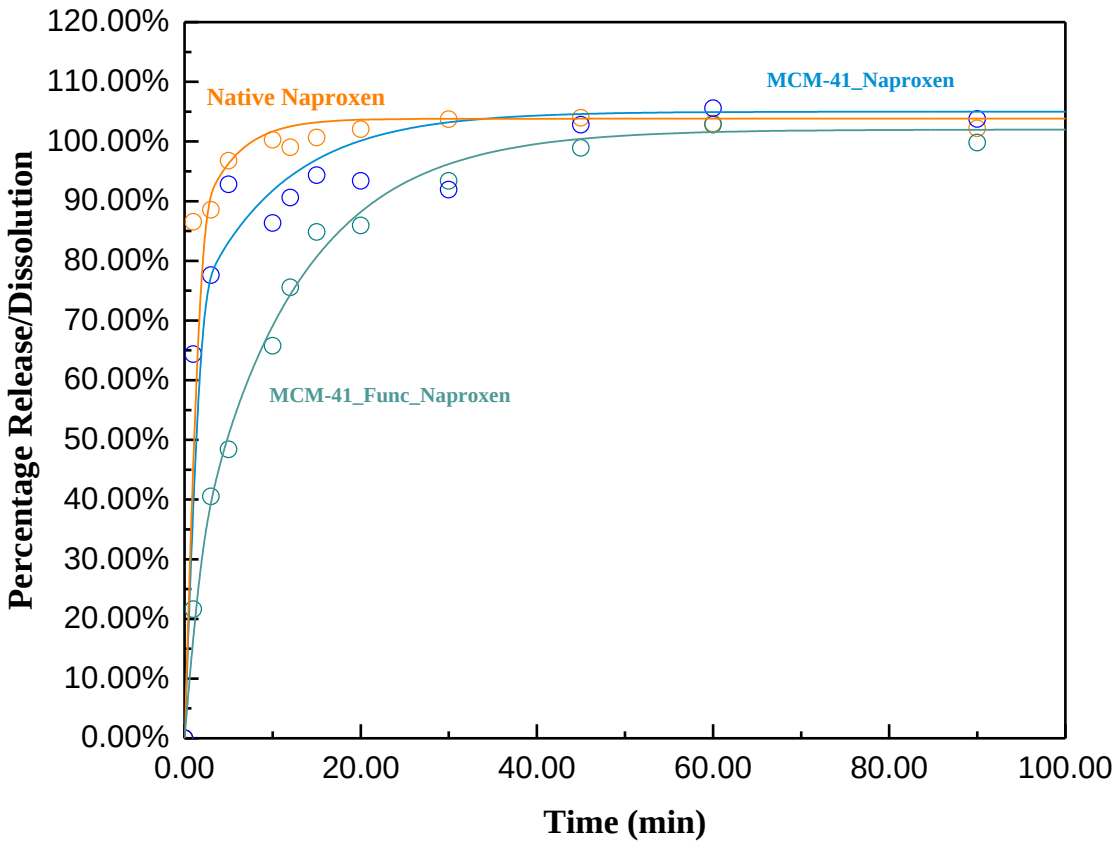

Figure 48. Normalized drug release and dissolution profiles in a pH= 6.8 media.

The results were normalized by the measurement at 24 hours. Native naproxen reaches about 100 % release in the first few minutes. In the first 20 minutes, the MCM-41 composite reaches about 90 % release, attaining a sort of plateau, which is only achieved above 45 minutes for the functionalized one. Therefore, a slower release rate occurs for the functionalized composite. This was not expected, as the drug should have fewer interactions with the silanol groups on the silica surface. However, these results are in good agreement with results from DRS, as the composite MCM-41 shows a higher mobility in the hydrated cycle than the functionalized one. One hypothesis is the higher water content in MCM-41_Naproxen exerting a stronger plasticizing effect in the incorporated drug and, therefore, promoting its release.

4 Conclusion

The pharmaceutical drug naproxen was investigated and its phase transformations were probed by calorimetry, showing that it is a highly crystallizeble drug. Under several thermal treatments amorphization was never reached for the native drug.

Aiming to obtain naproxen in the amorphous sate, incorporation in a solid host was used as a strategy. With this purpose, two different nanoporous silica matrixes were synthesized differing in their chemical surface composition: one unmodified MCM-41 and another MCM-41 with methyl capped groups (MCM-41_Func). This surface modification was confirmed by ATR-FTIR (enhancement of Si-O-Si and O-Si-O bands), TGA (mass loss above 350 ºC due to functional groups decomposition) and NMR (increase of siloxanes and emerging of Si-O-CH_3 groups). For morphological and textural characterization, SEM, TEM and nitrogen porosometry were used; a narrow pore size distribution centered in 3.0 and 2.9 nm was determined for, MCM-41 and MCM-41_Func, respectively.

Naproxen loading in the prepared matrixes was confirmed by a set of analytical methods such as ATR-FTIR, TGA, DSC, DRS and UV-Vis spectroscopy, which also allowed accessing its physical state.

Concerning thermal analysis, TGA evidenced an increase of thermal resistance for loaded naproxen. A wide glass transition was calorimetrically observed for both composites with onset at 9.33 ºC and midpoint at 17.49 ºC for MCM-41_Nap, and onset at 8.79 ºC and midpoint at 11.04 ºC for MCM-41_Func_Nap. The respective derivative was plotted, evidencing the existence of two populations, more distinguished, for MCM-41_Func_Naproxen, the one located at a higher temperature being the dominant one. The detection of a glass transition, confirms amorphization as indented. However, melting were always observed in both composites, the latter at a temperature close to the native drug and therefore, assigned to excess of naproxen outside pores. From the melting enthalpy, the crystallization degree was estimated as 6.59 % and 6.98 %, for the as prepared MCM-41_Nap and MCM-41_Func_Nap, respectively.

Moreover, a thermogram of MCM-41_Nap that didn’t show recrystallization, was collected two months later exhibiting only the glass transition, meaning that not just amorphization was achieved, but also it was possible to stabilize the amorphous form of

the highly crystallizable naproxen for at least this period.

By DRS, a technique to which the silica framework is insensitive, naproxen mobility was investigated in both composites in the frequency range from 10^{-1} to 10^{6} Hz and between -100 to 120 ºC. It was observed, by the shift to higher frequencies/lower temperatures, that the loaded drug becomes more mobile in the unmodified composite when hydrated. However, this is inverted in the dried samples, where incorporated naproxen shows a higher mobility for the functionalized composite, interpreted as weaker guest-host interactions. The study of loaded naproxen's mobility was taken more profoundly for the dried MCM-41_Naproxen composite, where isothermal spectra were analyzed to extract relaxation times. By extrapolation of the characteristic relaxation times to τ = 100 s, a dielectric glass transition was estimated, at 3.8ºC, revealing a good agreement with the T_g calorimetric value, confirming that the probed relaxation process is the one associated with the glass transition.

The drug release experiments demonstrate that 90% of the drug is released before forty-five minutes for any of the composites. Nonetheless, naproxen's release is faster in the hydrated unmodified composite, in good agreement with the mobility enhancement observed by dielectric spectroscopy. This complementary analysis provided a rational basis to understand and explain the observed drug release behavior.

These results, allowed concluding that naproxen/inorganic-silica show promising behavior as controlled drug delivery systems.

5 References

1. Di L, Kerns EH. *Drug-Like Properties: Concepts, Structure Design and Methods from ADME to Toxicity Optimization*.; 2016. doi:10.1016/C2013-0-18378-X.
2. Kümmerer K. Introduction: Pharmaceuticals in the Environment. In: *Pharmaceuticals in the Environment*. ; 2001. doi:10.1007/978-3-662-04634-0_1.
3. Williams H, Trevaskis N, Charman S, et al. Strategies to address low drug solubility in discovery and development. *Pharmacol Rev*. 2013;65(1):315-499. doi:10.1124/pr.112.005660.
4. Cordeiro T, Santos AFM, Nunes G, et al. Accessing the Physical State and Molecular Mobility of Naproxen Confined to Nanoporous Silica Matrixes. *J Phys Chem C*. 2016;120(26):14390-14401. doi:10.1021/acs.jpcc.6b04078.
5. Amaral MHAR. Estudo do Naproxeno em Formas de Aplicação Cutânea. Faculdade de Farmácia da Universidade do Porto.; 1997.
6. Takagi T, Ramachandran C, Bermejo M, Yamashita S, Yu LX, Amidon GL. A provisional biopharmaceutical classification of the top 200 oral drug products in the United States, Great Britain, Spain, and Japan. *Mol Pharm*. 2006;3(6):631-643. doi:10.1021/mp0600182.
7. Leuner C, Dressman J. Improving drug solubility for oral delivery using solid dispersions. *Eur J Pharm Biopharm*. 2000;50(1):47-60. doi:10.1016/S0939-6411(00)00076-X.
8. Griffin JP. *The Textbook of Pharmaceutical Medicine: 6th Edition*.; 2009. doi:10.1002/9781444317800.
9. Horter D, Dressman JB. Influence of physiochemical properties on dissolution of drugs. *Adv Drug Deliv Rev*. 1997;25(1):3-14. doi:10.1016/S0169-409X(96)00487-5.
10. Kawabata Y, Wada K, Nakatani M, Yamada S, Onoue S. Formulation design for poorly water-soluble drugs based on biopharmaceutics classification system: Basic approaches and practical applications. *Int J Pharm*. 2011;420(1):1-10. doi:10.1016/j.ijpharm.2011.08.032.
11. Basanta Kumar Reddy B, Karunakar A. Biopharmaceutics classification system: A regulatory approach. *Dissolution Technol*. 2011;18(1):31-37. doi:10.4103/0975-8453.59514.
12. Yu L. Amorphous pharmaceutical solids: Preparation, characterization and stabilization. *Adv Drug Deliv Rev*. 2001;48(1):27-42. doi:10.1016/S0169-409X(01)00098-9.
13. Einfal T, Planinšek O, Hrovat K. Methods of amorphization and investigation of

the amorphous state. *Acta Pharm*. 2013;63(3):305-334. doi:10.2478/acph-2013-0026.

14. Lukas K, LeMaire PK. Differential Scanning Calorimetry: Fundamental overview. *Resonance*. 2009;14(8):807-817. doi:10.1007/s12045-009-0076-7.
15. Moura Ramos JJ, Diogo HP. Are Crystallization and Melting the Reverse Transformation of Each Other? *J Chem Educ*. 2006;83(9):1389. doi:10.1021/ed083p1389.
16. Atkin P, Paula J. *Physical Chemistry*.; 2006. doi:10.1039/C1CS15191F.
17. Dsc TM. Introducing the Temperature Modulated DSC. 1993;(Figure 1):1-8.
18. Förster S, Schnablegger H, Rabe JP, et al. Makromolekulare chemie 1999. *Nachrichten aus der Chemie*. 2000. doi:10.1002/nadc.20000480315.
19. Debenedetti PG, Stillinger Frank H. Supercooled liquids and the glass transition. *Nature*. 2001;410(6825):259-267. doi:10.1038/35065704.
20. Clas S, Dalton C, Hancock B. Differential scanning calorimetry: applications in drug development. *Pharm Sci Technolo Today*. 1999;2(8):311-320. doi:http://dx.doi.org/10.1016/S1461-5347(99)00181-9.
21. Grün M, Unger KK, Matsumoto A, Tsutsumi K. Novel pathways for the preparation of mesoporous MCM-41 materials: Control of porosity and morphology. *Microporous Mesoporous Mater*. 1999;27(2-3):207-216. doi:10.1016/S1387-1811(98)00255-8.
22. Krasucka P, Goworek J. MCM-41 silica as a host material for controlled drug delivery systems. 2015;LXX.
23. Halamová D, Zeleňák V. NSAID naproxen in mesoporous matrix MCM-41: Drug uptake and release properties. *J Incl Phenom Macrocycl Chem*. 2012;72(1-2):15-23. doi:10.1007/s10847-011-9990-x.
24. Wu S, Wang J, Liu G, Yang Y, Lu J. Separation of ethyl acetate (EA)/water by tubular silylated MCM-48 membranes grafted with different alkyl chains. *J Memb Sci*. 2012;390-391:175-181. doi:10.1016/j.memsci.2011.11.034.
25. Díaz I, Márquez-Alvarez C, Mohino F, Pérez-Pariente J, Sastre E. Combined Alkyl and Sulfonic Acid Functionalization of MCM-41-Type Silica: Part 1. Synthesis and Characterization. *J Catal*. 2000;193(2):283-294. doi:10.1006/jcat.2000.2898.
26. Moritz M, Geszke-Moritz M. Mesoporous materials as multifunctional tools in biosciences: principles and applications. *Mater Sci Eng C Mater Biol Appl*. 2015;49:114-151. doi:10.1016/j.msec.2014.12.079.
27. Hofstetter H. FT-IR Spectroscopy Attenuated Total Reflectance FT-IR. 2007.
28. PerkinElmer. Thermogravimetric Analysis (TGA) A Beginner ' s Guide. *Analysis*. 2010:1-19.

29. Goldstein J, Newbury DE, Joy DC, et al. *Scanning Electron Microscopy and X-Ray Microanalysis*.; 2003. doi:10.1007/978-1-4615-0215-9.
30. Amemiya S, Bard AJ, Fan F-RF, Mirkin M V, Unwin PR. Scanning electrochemical microscopy. *Annu Rev Anal Chem (Palo Alto Calif)*. 2008. doi:10.1146/annurev.anchem.1.031207.112938.
31. Egerton RF. *Physical Principles of Electron Microscopy*.; 2005. doi:10.1016/S1369-7021(05)71232-3.
32. Storing C. Chapter 2 General experimental methods. 2015:35-47.
33. KV K, SR A, PR Y, RY P, VU B. Differential Scanning Calorimetry: A Review. *Res Rev J Pharm Anal*. 2014;3(3):11-22. http://www.rroij.com/open-access/differential-scanning-calorimetry-a-review-.php?aid=34700.
34. Bai S, Wang W, Dybowski C. Solid state NMR spectroscopy. *Anal Chem*. 2010;82(12):4917-4924. doi:10.1021/ac100761m.
35. Schwartz E, Blazewicz S, Doucett R, Hungate BA, Hart SC, Dijkstra P. Natural abundance δ15N and δ13C of DNA extracted from soil. *Soil Biol Biochem*. 2007;39(12):3101-3107. doi:10.1016/j.soilbio.2007.07.004.
36. Zhao XS, Lu GQ, Whittaker AK, Millar GJ, Zhu HY. 29 Si Comprehensive Study of Surface Chemistry of MCM-41 Using CP / MAS NMR , FTIR ,. 1997;5647(97):6525-6531.
37. Yasmin T, Müller K. Structural characterization of octadecyl modified MCM-41 silica by NMR and FTIR. *J Porous Mater*. 2016;23(2):339-348. doi:10.1007/s10934-015-0086-7.
38. Del Rosal I, Gerber IC, Poteau R, Maron L. Grafting of lanthanide complexes on silica surfaces dehydroxylated at 200 °c: A theoretical investigation. *New J Chem*. 2015;39(10):7703-7715. doi:10.1039/c5nj01645b.
39. Kremer F, Schoenhals A. *Broadband Dielectric Spectroscopy*.; 2002.
40. Agilent Technologies. Basics of Measuring the Dielectric Properties of Materials. *Appl Note*. 2006:1-32. doi:5989-2589EN.
41. Feldman Y, Gusev YA, Vasilyeva MA. Dielectric relaxation phenomena in complex systems - tutorial. 2012:134.
42. Brochier A, Aufray M, Possart W. Materials with Complex Behaviour II. 2012;16. doi:10.1007/978-3-642-22700-4.
43. Na. Ultraviolet -Visible Spectroscopy (UV). *Rsc*. 2014:68.
44. Soediono B. *Introduction*. Vol 53.; 2007. doi:10.1017/CBO9781107415324.004.
45. Vallet-Regí M, Izquierdo-Barba I, Colilla M. Structure and functionalization of mesoporous bioceramics for bone tissue regeneration and local drug delivery. *Philos Trans R Soc A Math Phys Eng Sci*. 2012;370(1963):1400-1421.

doi:10.1098/rsta.2011.0258.

46. Jin X, Wang Q, Sun J, Panezai H, Bai S, Wu X. Dual (pH- and temperature-) stimuli responsive nanocarrier with bimodal mesoporous silica nanoparticles core and copolymer shell for controlled ibuprofen-releasing: Fractal feature and diffusion mechanism. *Microporous Mesoporous Mater*. 2017;254:77-85. doi:10.1016/j.micromeso.2017.05.003.
47. WOOD DL, RABINOVICH EM, JOHNSON DW, MacCHESNEY JB, VOGEL EM. Preparation of High-Silica Glasses from Colloidal Gels: III, Infrared Spectrophotometric Studies. *J Am Ceram Soc*. 1983;66(10):693-699. doi:10.1111/j.1151-2916.1983.tb10531.x.
48. Morrow BA, McFarlan AJ. Surface vibrational modes of silanol groups on silica. *J Phys Chem*. 1992;96(3):1395-1400. doi:10.1021/j100182a068.
49. Allesø M, Chieng N, Rehder S, Rantanen J, Rades T, Aaltonen J. Enhanced dissolution rate and synchronized release of drugs in binary systems through formulation: Amorphous naproxen-cimetidine mixtures prepared by mechanical activation. *J Control Release*. 2009;136(1):45-53. doi:10.1016/j.jconrel.2009.01.027.
50. Emanuel H, Grundschober AF, Leuthold S, et al. *Functional Analysis of the Extracellular Cysteine Residues in the Human Organic Anion Transporting Polypeptide , OATP2B1*. Vol 63.; 2015. doi:10.1124/mol.105.019547.et.
51. Löbmann K, Laitinen R, Grohganz H, Strachan C, Rades T, Gordon KC. A theoretical and spectroscopic study of co-amorphous naproxen and indomethacin. *Int J Pharm*. 2013;453(1):80-87. doi:10.1016/j.ijpharm.2012.05.016.
52. Paroha S, Dubey RD, Mallick S. Physicochemical interaction of naproxen with aluminium hydroxide and its effect on dissolution. *Farmacia*. 2013.

6 Anexes

Calibration curves for dissolution/control release trials: